Characteristics and Origin of Glauconite in Drillcore PH010B from the Toolse Phosphorite Deposit, Leetse Formation

Bachelor thesis

Student: Kirke Britt Benjamin
Student code: 232927LARB
Supervisor: Rutt Hints, PhD, Senior Researcher –
Head of the division of Mineral Resources and Applied Geology: Department of Geology
Study programme: Earth systems, climate and technologies (LARB17-23)

Tallinn 2026

Glaukoniidi karakteristikud ja genees Leetse kihistus Toolse fosforiidimaardla puuraugus PH010B

Bakalaureusetöö

Üliõpilane: Kirke Britt Benjamin
Üliõpilaskood: 232927LARB
Juhendaja: Rutt Hints, vanemteadur, osakonnajuhataja –
Maavarade ja rakendusgeoloogia osakond: Geoloogia osakond
Õppekava: Maa süsteemid, kliima ja tehnoloogiad (LARB17-23)

Declaration

I hereby declare that I have written this thesis independently and the thesis has not previously been submitted for defence. All works and major viewpoints of the other authors, data from sources of literature and elsewhere used for writing this paper have been properly cited.

Author: Kirke Britt Benjamin
[Digitally signed]

The thesis complies with the requirements for bachelor's theses.

Supervisor: Rutt Hints
[allkiri ja kuupäev]

Table of Contents

Abstract

Glauconite is a K- and Fe-rich authigenic phyllosilicate forming in shallow marine shelf environments under conditions of low sedimentation rates and suboxic pore-water chemistry. In Estonia, glauconite is most developed within the Lower Ordovician Leetse Formation, where glauconite-rich sandstones occur in close stratigraphic association with phosphorite deposits across northern Estonia. Despite regional investigations of the Leetse Formation, the characteristics and genesis of glauconite within the Toolse phosphorite deposit have not previously been addressed through integrated high-resolution analysis. This study presents a systematic characterisation of glauconite from a one-metre interval from drillcore PH010B from the Toolse deposit, using scanning electron microscopy (SEM), X-ray diffraction (XRD) and X-ray fluorescence (XRF). SEM observations reveal glauconite as rounded to sub-rounded pellets (80-500 μm) with a downcore change in internal microstructures from flaky and porous textures in the upper interval to denser fibrous-lamellar groupings at the base. Mineralogical data confirms glauconite as the dominant mineral phase in the lower interval, with contents in the entire interval ranging from 14.6% to 78.5%. Geochemical analysis reveals a downcore increase in K_2O and Fe_2O_3. The combined dataset supports in situ authigenic glauconitisation from fecal pellet precursors under suboxic shelf conditions. The trace occurrence of pyrite despite high iron contents in whole rock analysis indicates that nearly all iron is structurally within glauconite, constraining the diagenetic environment to suboxic conditions. The vertical geochemical, mineralogical and microstructural gradient indicates variations in sedimentation rate and pore-water iron availability during Leetse Formation deposition, likely linked to episodes of sediment starvation on the Lower Ordovician Baltic shelf. As the study is based on a single drillcore, lateral variability across the Toolse deposit remains unassessed. Further studies could focus on incorporating additional boreholes combined with oriented clay mineral, trace element and isotopic analyses to constrain the structural evolution of glauconite and the diagenetic history of the deposit.

Glaukoniidi karakteristikud ja genees Leetse kihistus Toolse fosforiidimaardla puuraugus PH010B

Annotatsioon

Glaukoniit on K- ja Fe-rikas autigeenne kihtsilikaatne mineraal, mis moodustub madalamerelistes šelfikeskkondades aeglase settimise ja suboksilise poorivee olemasolu korral. Eestis on glaukoniit enim levinud Vara-Ordoviitsiumi Leetse kihistus, kus glaukoniidirikastes liivakivides esinevad üksikud savi- ja karbonaatkivimi vahekihid. Hoolimata piirkondlikest uuringutest, mis keskenduvad Leetse kihistule ja Toolse fosforiidimaardlale, ei ole sealse glaukoniidi karakteristikuid ja tekkemehhanisme varem integreeritud kõrglahutusliku analüüsi kaudu kirjeldatud. Käesolev bakalaureusetöö esitab süstemaatilise glaukoniidi iseloomustuse Toolse maardla puursüdamikust PH010B pärineva ühemeetrise intervalli põhjal, rakendades skaneerivat elektronmikroskoopiat (SEM), röntgendifraktsiooni (XRD) ja röntgenflurestsentsanalüüsi (XRF). SEM-vaatlused näitavad, et glaukoniit esineb läbilõikes ümardunud kuni poolümardunud teradena (80-500 µm), mille mikrostruktuurides esineb sügavuse kasvamisel muutus: ülemises osas domineerivad kihilisemad ja poorsed terad, alaosas aga tihedalt pakitud kiudjad-lamellaarsed struktuurid. Mineraloogilise andmestiku põhjal varieerub glaukoniidi sisaldus vahemikus 14.6% kuni 78.5% ning uuritud intervalli alumises osas on glaukoniit domineeriv mineraal. Geokeemilised andmed näitavad K_2O ja Fe_2O_3 sisalduse suurenemist sügavuse kasvades. Kombineeritud andmestik toetab autigeenset in situ glaukoniidistumist fekaalpelletite lähtematerjalist suboksilistes šelfitingimustes. Püriidi vähene sisaldus koos kõrge rauasisaldusega kogu kivimis viitab sellele, et kogu raud on struktuurselt glaukoniidis, piiritledes diageneetilise keskkonna suboksiliste tingimustega. Vertikaalne geokeemiline, mineraloogiline ja mikrostruktuurne gradient viitab settimiskiiruse ja poorivee rauasisalduse varieerumisele Leetse kihistu settimise ajal, tõenäoliselt seotud piiratud settematerjaliga Vara-Ordoviitsiumi Balti šelfil. Kuna käesolev uuring põhineb üksiku puursüdamiku andmestikul, jääb Toolse maardla glaukoniidi lateraalne varieeruvus hindamata. Edasised uuringud võiksid keskenduda täiendavate puuraukude kaasamisele koos suunatud savimineraalide, mikroelementide analüüside ja isotoopanalüüsidega, et täpsemalt määrata glaukoniidi struktuurset arengut Eesti geoloogilises kontekstis ja Toolse fosforiidimaardla diageneetilist ajalugu.

List of figures

1. Introduction

Glauconite is a characteristic mineral of shallow marine sedimentary successions and has long served as an indicator of depositional conditions, sedimentation rates and early diagenetic environments. Glauconite is a K- and Fe-rich phyllosilicate mineral that forms through authigenic processes at or near the sediment-water interface (Lopez-Quiros, 2020). The occurrence of glauconite is closely tied to conditions of sediment starvation, suboxic pore-water chemistry and prolonged residence time on marine shelf (Tribovillard, 2024). Glauconite is not only an important indicator of past oceanographic and depositional controls, it is also a mineral of growing economic interest, given its potential as potassium fertiliser and additives in water purification filters (Pihel, 2025; Spoljaric, 1978).

In Estonia, glauconite is a commonly occurring mineral in Lower Palaeozoic sedimentary successions and its most abundant occurrences are found within the Leetse Formation of the Hunneberg Stage (Early Ordovician). The glauconitic sandstones of the Leetse Formation extend laterally across northern Estonia and have been documented in boreholes and outcrops along the North Estonian Klint. Previous studies show that these deposits are mineralogically and geochemically variable, with glauconite contents ranging from a few percent to over 70% in the most enriched sections and potassium contents in purified glauconite reaching 5-9 wt% depending on the degree of maturation (Heinsalu, 1970). The Leetse Formation has also attracted attention in the context of Estonian phosphorite deposits, where glauconite-rich sandstones appear in close relation to phosphorite beds, reflecting shared depositional conditions during the Cambrian-Ordovician transition. Particularly, the Toolse deposit represents a notable Lower Ordovician phosphorite occurrence in Estonia and forms part of the broader Rakvere phosphorite-bearing region.

While the phosphorite beds of the Rakvere region have been extensively studied, the glauconite of the Toolse deposit has not been subjected to systematic, high-resolution investigation that combines morphological, geochemical and mineralogical data within a well-characterised stratigraphic framework. This gap limits the ability to interpret glauconite at Toolse as an indicator for depositional conditions and to evaluate its potential significance within the context of the Early Ordovician Baltic Palaeobasin.

This study addresses these gaps through an integrated, high-resolution characterisation of glauconite from a selected interval of drillcore PH010B, drilled in 2020 at the Toolse phosphorite deposit in northeastern Estonia. The studied interval spans approximately 1 metre within the Leetse Formation and captures the full range of glauconitic lithologies preserved in the core. The analytical programme combines scanning electron microscopy with energy dispersive spectroscopy (SEM-EDS) for pellet-scale morphological and compositional characterisation, X-ray diffraction (XRD) for semi-quantitative mineralogical analysis and X-ray fluorescence (XRF) for whole-rock major element geochemistry. These analyses provide complementary datasets that can be interpreted in an integrated manner.

The objectives of the study are to:

1. Characterise the external morphology, internal microstructures and surface features of glauconite pellets using SEM imaging;

2. Document the mineralogical composition and its vertical variation across the studied interval using XRD;
3. Determine the major element geochemical composition and identify systematic geochemical trends using XRF;
4. Use the combined dataset to assess the genesis, likely precursor materials, degree of maturity and early diagenetic conditions of glauconite evolution in the Toolse deposit;
5. Place the findings of the study within the broader framework of Leetse Formation glauconitisation and Early Ordovician depositional conditions in the Baltic Palaeobasin.

The results contribute new, deposit-scale insights into a mineral that has been recognised and studied, but not systematically at this level of resolution in the Estonian geological context. In doing so, the study provides a basis for more targeted future investigations of glauconite maturity, resource potential and depositional significance within the Leetse Formation, and adds to the growing body of work on authigenic mineral formation in Early Palaeozoic epicontinental shelf environments.

2. Literature review

2.1. Glauconite and its mineralogical characteristics

Glauconite is commonly described as a complex K- and Fe- rich green phyllosilicate belonging to the mica group. Its occurrence is predominantly related to marine sedimentary environments where it forms green pellets or grains (Lopez-Quiros, 2020; Krainer, 2022).

Structurally, glauconite is a dioctahedral 2:1 phyllosilicate consisting of tetrahedral-octahedral-tetrahedral sheets, with potassium in its interlayer sites. The crystal structure of the phyllosilicate presents characteristic substitutions of Al or Fe^{3+} in tetrahedral sites and octahedral trivalent cations. Generally, 5-12% of the total iron in glauconite is ferrous (Fe^{2+}), while the rest is ferric (Fe^{3+}). The general formula for the glauconite mineral can be given as:

$$K_{x+y}Si_{4-x}Al_x{\sim}4Fe^{3+}AlMgFe^{2+}{}_{\sim 2}O_{10}OH_2$$

where x ranges from 0.2 to 0.6 and y, which represents the sum of divalent octahedral cations, is between 0.4 and 0.6 (Huggett, 2005). However, extensive isomorphic substitutions in the tetrahedral and octahedral sheets, as well as in the interlayer space, make the composition of natural glauconite rather variable and complicates its classification and genetic interpretation (Hower, 1961).

Glauconite commonly occurs as a mixed layer mineral, with alternating illite- and smectite-like layers. During diagenetic maturation of such mixed layered phases, the proportion of illitic layers begins to increase (Thompson, 1975).

2.2 Genesis of glauconite

2.2.1. Depositional environments

Glauconite formation is associated with very low sedimentation rates in marine shelf environments. These environments are usually located on continental shelves and upper slopes and allow prolonged interaction between sediment particles and seawater, which is essential for the formation of authigenic minerals (Tribovillard, 2024; Rasis, 2022) (Figure 1). Such sedimentation conditions are linked to transgressive systems, where sediment starvation promotes authigenic mineral formation and the development of condensed intervals of sediments enriched in glauconitic material (Banerjee, 2015).

Suboxic to weakly reducing (ferruginous) conditions are considered essential for glauconitisation as they permit the coexistence of Fe^{2+} and Fe^{3+} required to incorporate into the structure of glauconite (Tribovillard, 2024). These conditions develop in microenvironments enriched in organic matter, such as within fecal pellets or sediment pore waters, where localized oxygen depletion enhances iron availability (Tribovillard, 2023).

Although previous studies and models of glauconitisation emphasize low-energy outer shelf settings, more recent studies have suggested that glauconite may form in a broader range of environments,

including shallow and higher-energy settings, provided that suitable geochemical conditions are present (Chafetz, 2000).

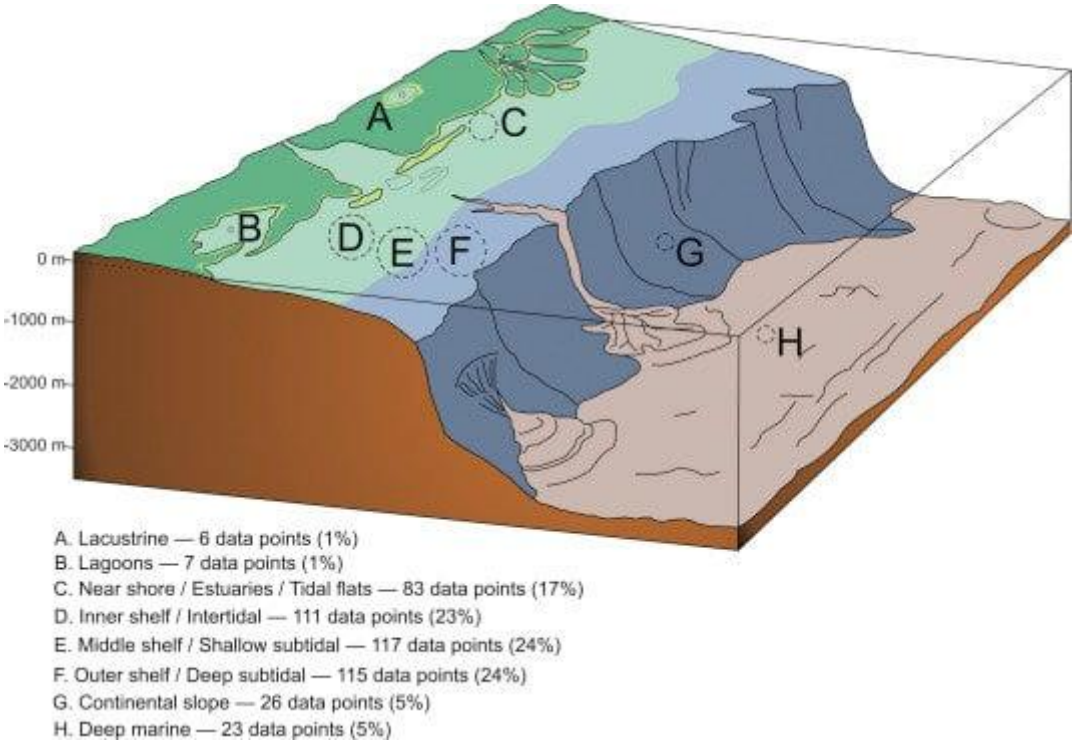

Figure 1. Glauconite occurences in different depositional environments (Banerjee, 2015).

2.2.2. Formation mechanisms

Glauconite is an authigenic mineral that forms at or near the sediment-water interface. Its formation involves early diagenetic processes, including dissolution, precipitation and recrystallization of precursor materials such as Fe (III)oxides, Fe-kaolinites and Fe-smectites (Lopez-Quiros, 2020).

Suggested precursors include fecal pellets and clay aggregates that undergo progressive chemical alteration, as well as bioclasts and detrital grains that act as substrates for mineral growth (Lopez-Quiros; Tribovillard, 2024). The transformation process typically begins with the formation of Fe-rich smectitic phases, which evolve through potassium incorporation and structural reorganization into glauconitic mica (Lopez-Quiros, 2020).

The extent to which glauconite forms through authigenic processes in contrast to being reworked remains a subject of debate. Some glauconite grains are interpreted as autochthonous and formed directly within the host sediment while others exhibit evidence of transport and redeposition, particularly in dynamic shelf environments. As a result, both in-situ growth and sedimentary reworking may contribute to the occurrence and distribution of glauconitic deposits (Krainer, 2022) (Figure 2).

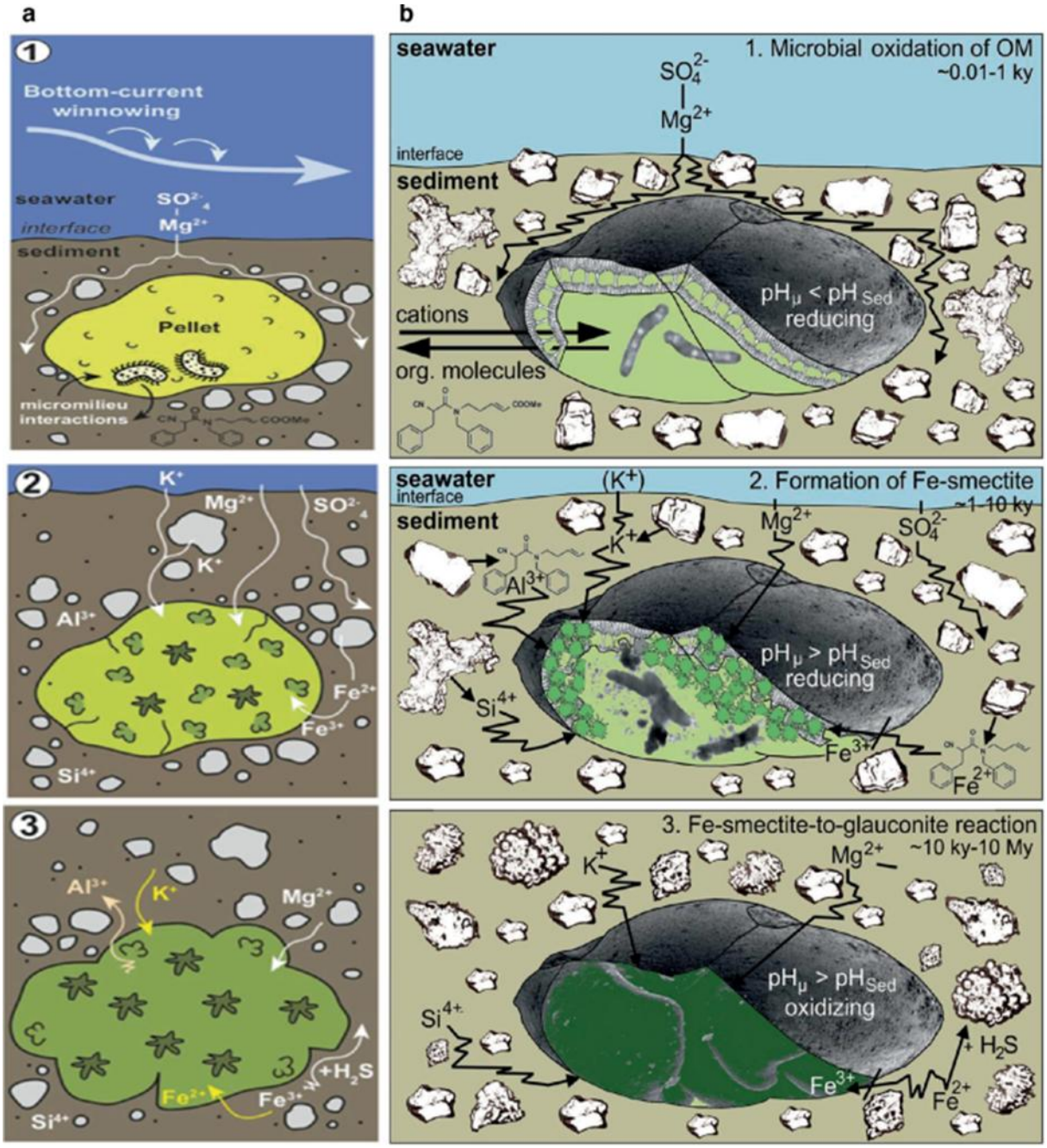

Figure 2. Conceptual model illustrating the formation and maturation of glauconite pellets in marine shelf sediments (El-Habaak, 2023).

2.2.3. Maturation and evolution

Glauconite maturation involves progressive potassium enrichment and structural ordering. During this process, Fe-rich smectitic precursors gradually incorporate K^+ into interlayer sites, leading to the development of a more ordered, mica-like structure (Rafiei, 2023; Lopez-Quiros, 2020).

Several authors distinguish between nascent, evolved and highly evolved glauconite based on K_2O content and crystallinity. These stages are meant to reflect increasing degrees of chemical and structural maturity, with higher potassium content corresponding to more evolved stages of glauconitisation (Tiyana, 2022).

The stages of glauconite evolution are often interpreted as reflecting residence time at the sediment-water interface (Tiyana, 2022). Prolonged exposure to seawater facilitates continued ion exchange and mineral growth, allowing glauconite grains to evolve over timescales ranging from thousands to millions of years. Thus, glauconite maturity is widely used as an indicator of sedimentation rates and depositional conditions (Rafiei, 2023).

2.2.4. Geochemical aspects

The incorporation of potassium is a key aspect of glauconite evolution and is influenced both by environmental and diagenetic factors. Potassium uptake occurs primarily through exchange with seawater and is essential for the transformation of smectitic precursors into glauconitic mica (Lopez-Quiros, 2020). The availability of K^+ and the duration of water-sediment interaction strongly influence the degree of maturation (Tribovillard, 2024).

Iron also plays a central role in glauconite formation. Iron occurs both as ferrous and ferric states, reflecting fluctuating redox conditions during formation. The coexistence of these oxidation states is indicative of suboxic to mildly reducing environments and is essential for the development of the glauconite structure (Tribovillard, 2024).

Recent studies hypothesise that microbial processes may contribute to glauconite formation, but their role remains under debate. Microbial activity may facilitate the formation of Fe-rich precursor phases and influence redox conditions through the degradation of organic matter, thereby indirectly promoting glauconitisation (Lopez-Quiros, 2020).

2.3 Morphology of glauconite

Glauconite occurs as rounded to sub-rounded microcrystalline aggregates or pellets, often interpreted as altered fecal material. These pellets are referred to as peloids and they represent the most characteristic form of glauconite in sedimentary rocks and are widely observed in marine shelf deposits (Krinsley, 1998; Lee, 1997). In addition to spheroidal shapes, glauconite grains may also exhibit ovoid, ellipsoidal or irregular morphologies which reflect both their precursor material and subsequent diagenetic modification (Krinsley, 1998). The previously mentioned irregular morphologies have been demonstrated and identified in earlier studies by Triplehorn (1966) as tabular and discoidal, mammillated, vermicular, composite and fossil-replacement form (Figure 3).

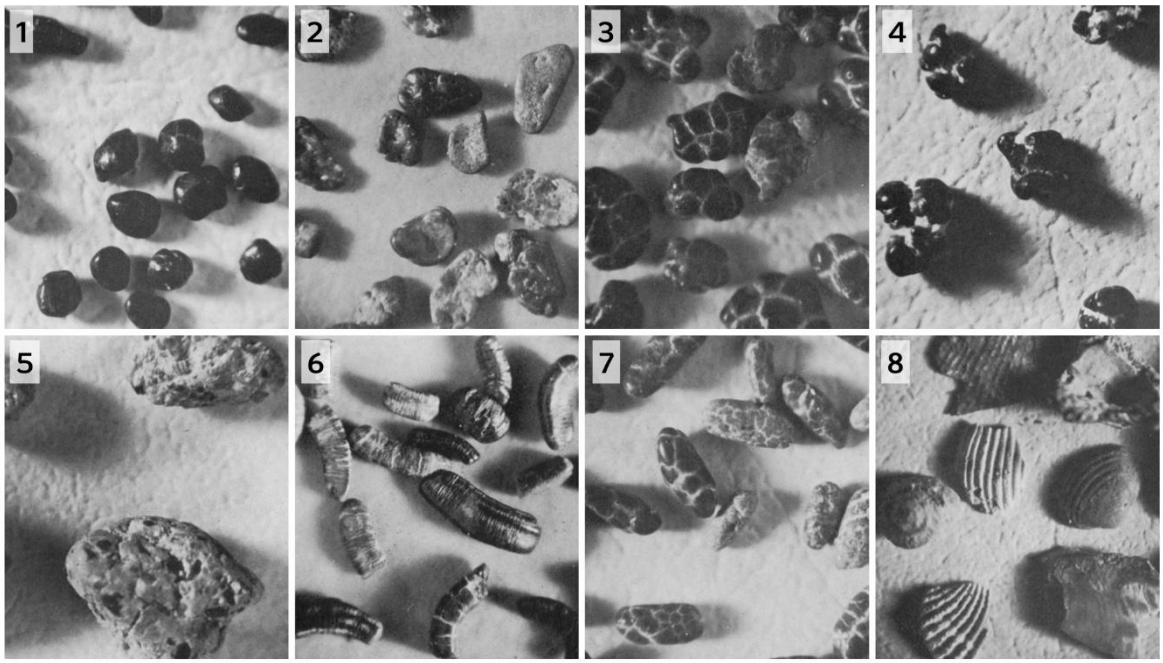

Figure 3. Morphological varieties of glauconitic pellets. 1 - spheroidal or ovoidal; 2 - tabular or discoidal; 3 - mammillated; 4 - lobate; 5 - composite; 6 - vermicular; 7 - capsule-shaped; 8 - fossil replacements or internal molds (Triplehorn, 1966).

Internal textures of glauconite aggregates range from homogeneous to finely laminated or zoned structures. Homogeneous pellets are associated with more advanced stages of glauconitisation, while heterogeneous or zoned textures may indicate incomplete transformation of multiple phases of mineral growth (Thompson, 1975). Random microcrystalline textures are considered the most common internal structure and may result from recrystallisation or alteration of clay-rich precursor material (Triplehorn, 1966). In some cases, internal features such as shrinkage cracks, fractures or infilled voids can be observed, which often indicate dehydration, compaction or later diagenetic processes (Lee, 1997).

Surface features of glauconite pellets can vary significantly, ranging from smooth, well-rounded grains to irregular, fissured or cracked surfaces. Smooth, compact grains are generally regarded as more mature and stable. Fissured or cracked surfaces may reflect ongoing diagenetic alteration or post-depositional modification (Krinsley, 1998). Additionally, coatings or rims of glauconitic material may develop on grains or bioclasts, related to authigenic growth within pore spaces or at grain boundaries during early diagenesis (Chafetz, 2000).

Morphological characteristics are often used to describe the degree of maturity and formation conditions of glauconite. For example, grain size, shape, internal homogeneity and degree of rounding have been linked to the duration of residence at the sediment-water interface, as well as to sedimentary energy conditions and reworking processes. Still, morphological interpretations must be supported by mineralogical and geochemical data, as similar external forms may correspond to different compositional or genetic stages (Burst, 1958).

2.4 Analytical methods for glauconite studies

2.4.1. Macro- and microanalytical methods

Glauconite and glauconite-bearing sedimentary rocks are studied by implementing a combination of macro- and microanalytical techniques. Because the mineralogical and chemical characteristics of glauconite vary, integrated analytical methods are required to define its morphology, mineral composition, crystallinity and geochemical variability. Commonly applied methods include X-ray diffraction (XRD), X-ray fluorescence (XRF), scanning electron microscopy (SEM) and petrographic analysis. Combined, these methods provide complementary information glauconitic material.

2.4.2. X-ray diffraction

X-ray diffraction (XRD) is a crystallographic analysis technique that provides information on the phase composition and structural arrangement of crystalline materials. The method is built on the interaction between incident X-rays and the periodic lattice planes within a crystal. Constructive interference occurs when the path difference between reflected X-rays satisfies Bragg's law ($n\lambda = 2d \sin\theta$), producing a diffraction pattern that characterizes the material's atomic structure. Each crystalline phase generates a unique set of diffraction peaks, allowing phase identification through comparison with reference databases. In addition to qualitative phase identification, XRD enables quantitative phase analysis, determination of crystallite site, preferred orientation and residual stress. However, factors such as absorption, scattering and fluorescence can affect peak intensity and background, which calls for careful interpretation of diffractograms (Emrich, 2013).

2.4.3. X-ray fluorescence

X-ray fluorescence (XRF) is a non-destructive analytical technique used to determine the elemental composition of materials based on the emission of characteristic X-ray radiation. When a sample material is irradiated with primary X-rays, inner-shell electrons may be ejected if the incident energy exceeds their binding energy. The resulting electronic vacancies are filled by electrons from higher shells, and the excess energy is released as secondary i.e. fluorescent X-rays with element-specific energies, enabling qualitative and quantitative analysis. The intensity of these emitted X-rays is proportional to the concentration of the corresponding elements, although matrix effects such as absorption and secondary fluorescence must be considered, as they influence signal attenuation and enhancement within the sample. XRF spectrometers typically operate in either energy dispersive (EDXRF) or wavelength-dispersive (WDXRF) modes, both of which allow rapid, precise and reproducible compositional analysis across a wide range of elements and concentrations (Brouwer, 2010).

2.4.4. Scanning electron microscopy

Scanning electron microscopy (SEM) is a high-resolution imaging technique that utilizes a focused electron beam to investigate surface morphologies and composition of samples. When the electron beam interacts with the sample, multiple signals are generated, including secondary electrons (SE) and backscattered electrons (BSE), which are fundamental to image formation. Secondary electrons are low-energy electrons emitted from the near-surface region and are primarily used for high-resolution topographic imaging due to their sensitivity to surface features (Kannan, n.d.). In contrast, backscattered electrons are high-energy electrons elastically scattered from deeper within the sample.

Their intensity if strongly dependent on the atomic number, making BSD imaging suitable for compositional contrast, where heavier elements appear brighter (Kannan, n.d.). SEM requires careful sample preparation to ensure accurate imaging. Common procedures include dehydration, mounting and coating the sample with a conductive layer such as gold to prevent charging under the electron beam (Pandey, 2025). For geological and mineralogical samples, resin embedding is frequently used to stabilize porous or fragile materials and allow polishing to a flat surface suitable for electron interaction (Grundmann, 2015).

2.5 Geological background

2.5.1. Baltic Palaeobasin and Ordovician stratigraphy

Estonia, the northernmost of the three Baltic states, is geologically located in the northwestern part of the East-European Platform, on the southern slope of the Fennoscandian Shield (Raukas, 1997). The crystalline basement of Estonia is covered by a relatively thin, monocline-dipping succession of Neoproterozoic and Lower Palaeozoic sedimentary rocks. The basement itself consists of intensely metamorphosed and deformed Precambrian crystalline rocks that belong to the Svecofennian Domain of the Fennoscandian Shield (Kirs, 2009).

The Ordovician Period describes the geological interval from 485 to 444 million years ago and is characterised by the dominance of seas, with land forming only 5-10% of the Earth's area (Nestor, 2007). The vast seas allowed for major taxonomic groups to appear or become more common and planktic and benthic faunas became increasingly more biogeographically differentiated (Raukas, 1997).

During the Ordovician Period, Estonia was part of the Baltica palaeocontinent, which drifted from high southern latitudes toward equatorial regions as a result of plate tectonic movement (Cocks, 2005). The Estonian area formed part of the extensive Baltoscandian Palaeobasin, a shallow epicontinental sea characterized by low-relief topography and widespread carbonate sedimentation under relatively stable tectonic conditions. Sedimentation during the Early Ordovician was dominated by slow accumulation of terrigenous, carbonaceous and glauconitic deposits on the shelf of the Baltica craton, with facies differentiation gradually increasing through time (Edward, 2022). As Baltica moved into lower latitudes, carbonate production intensified and extensive carbonate shelf environments developed across the basin. During the Middle and Late Ordovician, the basin evolved into a differentiated carbonate platform system with notable shelf and basin facies belts, combined with increased biological productivity and reef development (Penny, 2021).

The Ordovician succession of marine terrigenous and carbonate rocks in Estonian ranges from 70 to 180 m in thickness and extends from the Tremadocian to the Hirnantian. The Estonian Lower Ordovician succession is made up of the following stages: Pakekort, Varangu, Hunneberg, and Billingen. The glauconitic sandstones of Estonia belong to the Hunneberg Stage, an Early Ordovician stratigraphic unit that was initially defined in Sweden in 1956. Later, the unit was recognized as a distinct stage in the East Baltic region. In norther Estonia specifically, the Hunneberg Stage is characterized by poorly lithified, glauconitic terrigenous sediments, which form the lower part of the Leetse Formation (Raukas, 1997).

The stage has a maximum thickness of 4 m in northwestern Estonia, with the average thickness being less than 2 m and it consists of two main glauconitic units. The Klooga Member, which is made up of glauconitic siltstones (up to 2.9 m. thick) with dominating quartz and subordinate glauconite. Above the Klooga Member, the Joa Member consists of glauconitic siltstones and sandstones (up to 1.2 m. thick) that are strongly enriched in glauconite (50-70%), with quartz making up only about 10-20% (Raukas, 1997).

The base of the Hunneberg Stage is well defined with a lithological boundary consisting of glauconitic sands and silts laying conformably on underlying dark argillites of the Türisalu Formation or light-grey mudstones of the Varangu Formation (Raukas, 1997).

2.5.2. Glauconite in Estonia

Glauconite is a common mineral in Lower Palaeozoic sedimentary successions in Estonia, particularly within the Lower Ordovician deposits. Glauconite is most prominently present in the Leetse Formation of the Hunneberg Stage, where glauconite-rich sandstones have developed laterally across northern Estonia. These glauconite deposits are typically composed of siltstones and sandstones containing quartz and glauconite. The enriched intervals can contain up to 50-70% glauconite with lower successions typically showing a higher glauconite content (Heinsalu, 1970). The Leetse Formation is lithologically variable both vertically and laterally, which points to differences in hydrodynamic conditions, sediment influx, and depositional continuity across the basin. Studies of the formation along the North Estonian Klint indicate that the western sections are affected more by redeposition and winnowing processes, while the eastern sections preserve more homogeneous and stratigraphically complete glauconitic successions deposited under continuous shallow-marine conditions (Viira, 2006).

Previous studies on Estonian glauconite deposits have primarily focused on the mineralogical and geochemical characteristics of the mineral and are often carried out in the context of resource evaluation. Early work (Anso, 1947) demonstrated that Estonian glauconite has a variable composition and is often diluted by significant amount of quartz and carbonate material, which strongly influences bulk geochemical analyses (Anso, 1947). As a result, reported potassium contents in purified glauconite from glauconite-bearing sediments range between 5-8 wt%, although lower values are typical in bulk samples due to dilution effects (Heinsalu, 1970). These early findings are consistent with more recent studies, which indicate that glauconitic sandstones in the Leetse Formation typically contain 2-7% potassium, reflecting the mineralogical heterogeneity and varied maturation stages (Pihel, 2026). Notably, XRD and SEM-based analyses of separated glaucony grains from the Leetse Formation have identified potassium rich glauconite varieties, where K2O contents approach or even exceed 9 wt%, suggesting mature glauconite phases in certain intervals (Viira, 2006).

Geochemical analyses characterize Estonian glauconite by high Fe and moderate K contents, which is consistent with its classification as a K- and Fe- rich phyllosilicate. However, detailed studies reveal notable variability in major element composition, particularly SiO_2, Fe_2O_3, Al_2O_3, and K_2O. The compositional variability reflects both primary depositional conditions and post-depositional alteration processes. Studies of the Leetse Formation have also demonstrated regional geochemical differences within the basin. Glauconite obtained from the eastern areas of the North Estonian Klint

generally contains higher K_2O and Fe_2O_3 contents compared to glauconite in the western sections, suggesting lower and more continuous sedimentation conditions in the eastern part of the basin (Viira, 2006).

2.5.3. Geology of the study area

The study targets glauconitic sandstones of the Leetse Formation from the area of the Toolse phosphorite deposit, NE Estonia. The Toolse phosphorite deposit represents one of the major Lower Ordovician phosphorite occurrences in Estonia and is a part of the broader Rakvere phosphorite-bearing region, encompassing the Aseri and Rakvere deposits (Puura, 1987). This regional differentiation is essential, as it frames Toolse not as an isolated accumulation but a component of a laterally extensive, genetically linked phosphorite-black shale system that has developed along the northern margin of the East European Platform (Figure 4).

From a stratigraphic and lithological perspective, the Toolse deposit is characterized by phosphorite beds associated with a succession of siliciclastic and carbonate rocks. The phosphorite layer is overlain by metalliferous black shales, mudstones and glauconitic sandstones and limestones indicating a vertically evolving sedimentary environment (Teedumäe, 1990). The occurrence of homogeneous glauconite-rich intervals within the Leetse Formation suggests conditions of low sedimentation rates and prolonged residence time at or near the sediment-water interface, which are beneficial for both phosphogenesis and glauconitisation (Viira, 2006).

Phosphorite accumulation in the Rakvere region, including Toolse, was strongly controlled by the palaeotopography and sedimentary dynamics during the Cambrian-Ordovician transition. Irregularities in the underlying substrate, included elevated areas or bottom swells, influenced both the thickness and distribution of phosphorite beds. The depositional and structural conditions present imply that phosphorite formation was not uniform but spatially heterogeneous, with localised zones of enhanced accumulation (Heinsalu, 1994).

Previous studies of the Rakvere phosphorite region highlight that phosphorite formation was most intense during specific intervals of Early Ordovician sedimentation, correlating to particular biostratigraphic zones. This suggests that broader oceanographic and geochemical conditions, such as nutrient supply, redox state and biological productivity played an important role during phosphogenesis. In this context, glauconite beds that postdate these extensive phosphorite-forming episodes may serve as an additional proxy for deciphering the evolution of depositional conditions (Heinsalu, 1994).

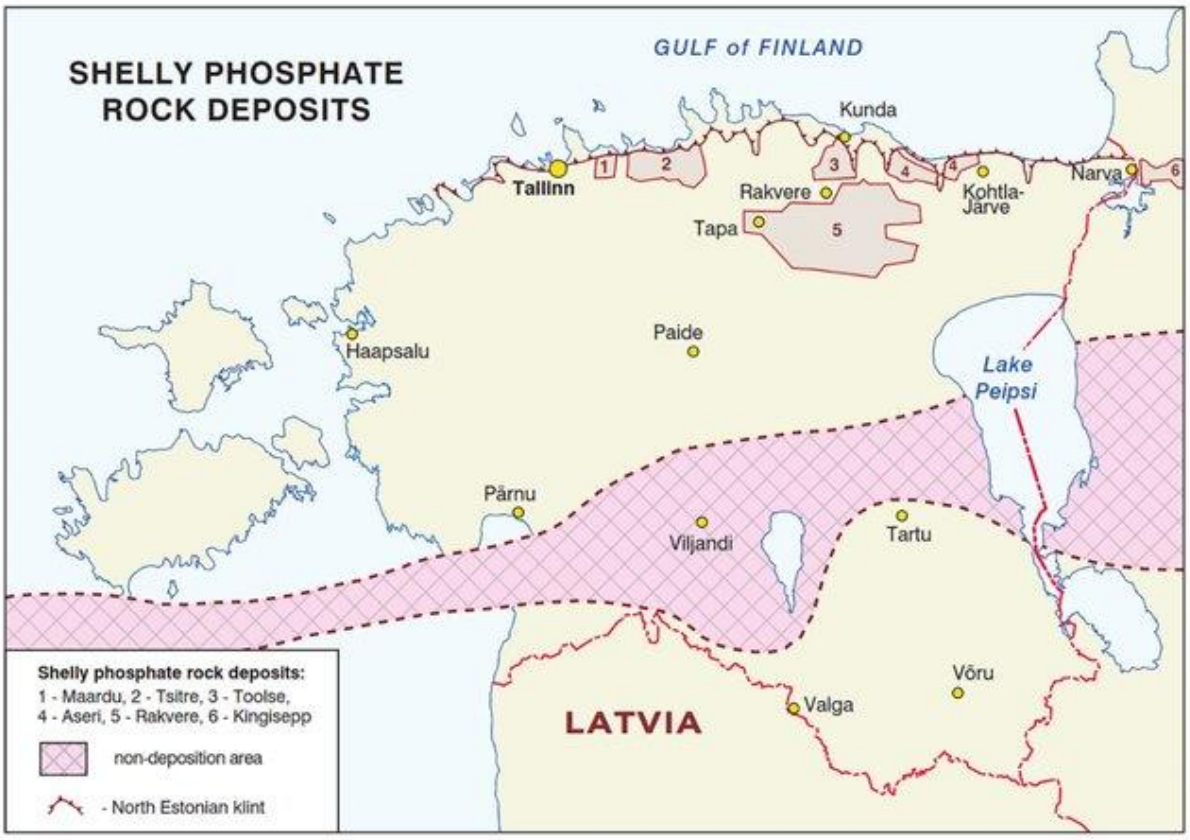

Figure 4. Distribution of shelly phosphorite deposits in Estonia (Bauert, 2015).

3. Knowledge gaps and research aim

Despite extensive geological investigation of Estonian phosphorite deposits, including the Toolse deposit, uncertainties remain regarding the characteristics and genesis of glauconite from the Leetse Formation in the area. Previous research has mainly focused on regional stratigraphy, phosphorite distribution and bulk geochemical properties, with glauconite often treated as an accompanying component rather than a primary subject of detailed analysis. This has resulted glauconite being described only in generalized terms, while its mineralogical complexity and lithological associations have not been systematically addressed. Moreover, detailed investigations of glauconite morphology—including pellet shape, internal textures and surface features—as well as stratigraphic and spatial variability of glauconite composition, remain limited, despite the recognized importance of these features for interpreting glauconite genesis.

A key limitation of existing studies is the lack of integrated high-resolution case studies that map morphological, mineralogical and geochemical variations of glauconite within well-characterised lithostratigraphic sections. Although techniques such as XRD, XRF, SEM and petrography have been applied in glauconite research in Estonia, there is limited information available linking glauconite characteristics with bulk-rock compositional and lithological variations in well-studied sections. This limits the ability to predict of range of glauconite properties variations associated both with small-scale lithological changes, phosphatic intervals and other depositional features, as well as variations at the broader deposit scale. In the Toolse deposit, glauconite-rich intervals are well documented, yet the geological interpretation on the origin, degree of maturation and diagenetic evolution of glauconite remains insufficient. Specifically, the processes of in situ glauconitisation and reworking processes have not been clearly resolved, nor has the relationship between glauconite properties and depositional conditions within the Early Ordovician Baltic Palaeobasin been fully established.

Considering this, the study provides an integrated high-resolution characterisation of glauconite within the Toolse phosphorite deposit based on detailed analysis of glauconite-rich section from drillcore PH010B. The work examines glauconite morphology—including pellet shape, size and internal microstructures—using scanning electron microscopy combined with energy dispersive spectroscopy, to assesses variability and maturity of glauconite phases. These interpretations are combined with whole rock mineralogical and geochemical data based on XRD and XRF analyses to evaluate variations and the degree of glauconitisation. By relating glauconite distribution to sedimentological boundaries, the study explores links between glauconite characteristics and depositional features. The combined datasets are used to assess the genesis of glauconite and reconstruct the depositional and early diagenetic conditions in the Toolse deposit area within the broader framework of the Ordovician Baltic Palaeobasin.

4. Methodology

4.1. PH010B borehole data

The study and analysis of Estonian glauconite characteristics is based on material from the Toolse PH010B borehole, drilled in 2020 in northeastern Estonia (59.468242°N, 26.452781°E) (Figure 5). The drillcore was selected due to well-defined sedimentary variations preserved within the Leetse Formation. The total depth of the borehole is 29.15 m, extending stratigraphically from the Väo Formation at the top to the Tiskre Formation at the base.

Figure 5. Location of the PH010B drillcore and study area in northeastern Estonia.

Drillcore PH010 provides a record of multiple sedimentary units, which include glauconite bearing intervals relevant to this study and analysis. A macroscopic core description was conducted to identify the lithology, sedimentary features and distribution of glauconitic material in the core. Lithological description acted as a basis for sampling.

4.2. Sampling process and resolution

Following the macroscopical description of the drillcore the core was first cut longitudinally into two halves using a wet saw. During cutting, the lower, weakly cemented part of the Leetse Formation proved relatively brittle, resulting in one half being less intact than the other. Both halves were photographed and evaluated for completeness. Based on this assessment, the more fragmented half was used for further analytical studies, while the more intact half was preserved as archival material in the core boxes for future studies (Figure 6).

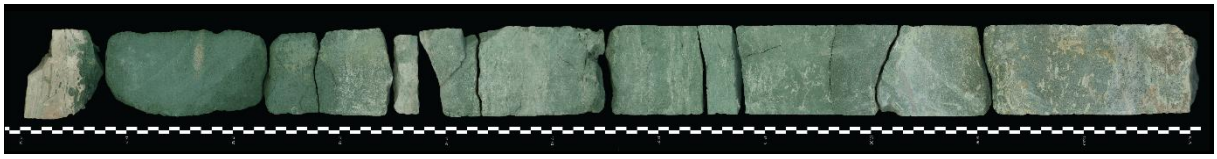

Figure 6. Preserved archival material from drillcore PH010B.

The selected half of the core was subsequently cut along its length to produce two quarters, each titled as A and B. This division was necessary to separate the analytical workflow into two main categories.

Quarter A was used for petrographic and microscopic analyses, which included scanning electron microscopy. Quarter B was allocated for the whole rock geochemical and mineralogical analyses.

The initial sample resolution was set at 5 cm intervals, but this was later adjusted to account for the irregular lithological boundaries and contact zones within the core. In total, 19 samples were collected. The samples were cut horizontally according to the defined sampling resolution to ensure consistency (Figure 7). Table 1 shows the final sampling intervals accompanied by the analytical methods applied to each interval (Table 1).

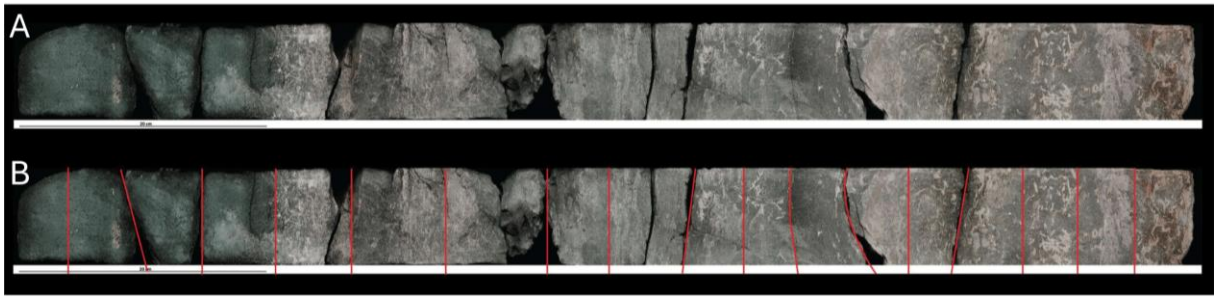

Figure 7. Core section selected for detailed sampling and analysis from drillcore PH010B. (A) Photograph of the sampled drillcore half; (B) Sampling intervals used for analyses (Photographs by Baranov, G.).

Table 1. Sampling intervals, subsample preparation and analytical methods applied.

Sample interval (m)	Thickness (cm)	Subsamples prepared	XRF	XRD	SEM-BSD	SEM-SED
16.70–16.75	5	KBB25-001 A/B	✓	✓	–	–
16.75–16.80	5	KBB25-002 B	✓	✓	✓	✓
16.80–16.84	4	KBB25-003 B	✓	✓	–	–
16.84–16.89	5	KBB25-004 B	✓	✓	–	–
16.89–16.93	4	KBB25-005 A/B	✓	✓	✓	✓
16.93–16.97	4	KBB25-006 B	✓	✓	–	–
16.97–17.02	5	KBB25-007 A/B	✓	✓	✓	✓
17.02–17.06	4	KBB25-008 B	✓	✓	–	–
17.06–17.10	4	KBB25-009 B	✓	✓	–	–
17.10–17.16	6	KBB25-010 A/B	✓	✓	✓	✓
17.16–17.23	7	KBB25-011 B	✓	✓	–	–
17.23–17.31	8	KBB25-012 B	✓	✓	–	–
17.31–17.38	7	KBB25-013 A/B	✓	✓	✓	✓
17.38–17.46	8	KBB25-014 B	✓	✓	–	–
17.46–17.55	9	KBB25-015 B	✓	✓	–	–
17.55–17.60	5	KBB25-016 A/B	✓	✓	✓	✓
17.60–17.65	5	KBB25-017 B	✓	✓	–	–
17.65–17.70	5	KBB25-018 A/B	✓	✓	✓	✓
17.70–17.72	2	KBB25-019 B	✓	✓	–	–

For petrographic and microscopical analyses (quarter A), representative intervals were selected to characterise the major lithological changes within of the core. This resulted in a selection of seven samples to reflect the major lithological sections present in the core.

For geochemical analyses (quarter B), the samples were prepared following the standard laboratory procedure of crushing the material with a jaw crusher and subsequently milling the material with a

fine sample grinder. This procedure produced a homogenous powder across the interval of each sample, suitable for XRD and XRF analysis. Prior to XRF analyses, loss on ignition at 950°C (LOI 950°C) was determined for each sample.

4.3 SEM analysis methodology

The selected samples were prepared in two ways, depending on the aim of the analysis. For internal structure and elemental composition analysis with backscattered electron detector (SEM-BSD), samples were cut to size, embedded in epoxy resin and polished, to produce a standard size mount suitable for analysis.

Preparation process included the following steps:

1. The selected sample intervals were cut into appropriate size (1.5cm x 1.5cm) using a wet saw;
2. Samples were placed in a silicone mold and impregnated with epoxy resin. The epoxy resin used was a mixture of Technovit 4006 SE powder and Technovit 4006 SE liquid, which is a fast curing resin and allowed for quick sample preparation process;
3. Once the sample was cured, the material was removed from the mold and the sample surface was polished to ensure a flat surface suitable for high-resolution imaging.

For morphological analyses with secondary electron detector (SEM-SED), the embedded mounts as well as three grain samples were coated with gold/palladium coating.

Scanning electron microscope studies were conducted using Semplor NANOS desktop SEM equipped with energy dispersive spectrometer. Depending on the working regime and the type of analysis, the accelerating voltage used for the beam was 10-15 kV, and the point size varied from 6 to 9.

4.4 XRD analysis methodology

The process of sample preparation for XRD analysis included the following procedures:

1. Approximately 0.1 g of powdered sample material was weighed into a mortar and ground with a pestle to produce a fine and uniform powder;
2. The powdered sample material was transferred onto a glass sample holder, and approximately 0.1 grams of ethanol was added;
3. The mixture was homogenized and evenly distributed across the surface of the sample holder;
4. The sample was ready for analysis once the ethanol had evaporated from the mixture (this was achieved by placing the holder into a laboratory oven for a short period of time or letting the mixture dry out at room temperature).

Once prepared, the samples were analysed using a Bruker D8 ADVANCE Bragg-Brentano X-ray diffractometer. To obtain a semiquantitative distribution of the crystalline phases, data treatment based on Rietveld refinement was further used.

4.5 XRF analysis methodology

For X-ray fluorescence, two preparation methods were used: pressed powder pellets and fused beads.

4.5.1 Pressed powder method

The process of preparing pressed powder discs comprised of the following procedures:

1. 8-8.5 grams of powdered material was weighed into a mortar, with the average amount used in this study being 8.4 g;
2. A binding agent (glue Mowiol) was added gradually with a syringe. The amount of binding material was adjusted according to the adhesive properties of the sample material;
3. The sample material and binding agent were ground in the mortar with a pestle 2-4 times to ensure the homogenization of the material.
4. The resulting mixture was placed into a press tool and compressed under a pressure of 5 tons;
5. The pellet was removed from the press tool, labelled with the sample identifier and dried in a laboratory oven at 105 °C for a minimum of 1 hour.

4.5.2 Fusion method

The preparation of fusion beads followed these steps:

1. A ceramic crucible was weighed using a Mettler Toledo scale;
2. 1 g of oxidised sample powder and 10 g of lithium borate flux were weighed into the crucible and thoroughly homogenized;
3. The mixture was transferred to a platinum crucible and fused using a Claisse M4 fusion instrument;
4. The fused melt was casted to produce a fusion bead and labelled with the sample identifier.

Once prepared, the samples were analysed using a Bruker S4 Pioneer wave dispersive X-ray spectrometer.

5. Results

5.1 Drillcore description and lithology

Figure 8 displays the interval between 16.75 and 17.75 m in drillcore PH010B (Figure 8). In the studied section of the Leetse Formation is dominated by a fine-grained glauconitic sandstone showing notable internal variability in texture, structure and glauconite distribution. The sandstone sections are generally well-sorted and composed of abundant glauconite grains, mostly occurring as rounded to sub-rounded pellets typically less than 0.5 mm in diameter. The glauconite content can be described as high throughout the interval, with the relative contents increasing downcore.

The upper part of the interval (16.7-17.15 m) is characterized by carbonate cementation and structural complexity. Weak horizontal layering is present, combined with mottled textures, indicating bioturbation. In this section, glauconite occurs both as individual pellets and irregularly enriched patches or masses.

In the lower part of the interval (17.15-17.7 m) the glauconitic sandstone becomes more uniform in texture with abundant glauconite and minor carbonate cement. Due to poor sedimentation this interval is rather friable. Glauconite pellets in this section appear well developed and evenly distributed. Associated mineral phases and bioturbation are less evident downcore.

Throughout the entire interval, except for the contact between Leetse glauconitic sandstone and Varangu mudstone and between above-described intervals, the lithological changes are generally gradational, and no well-defined boundaries can be observed. Overall, the studied interval can be characterized by a high glauconite content, fine grain size and variable internal structures, which include bioturbation, weak lamination, and localized cementation.

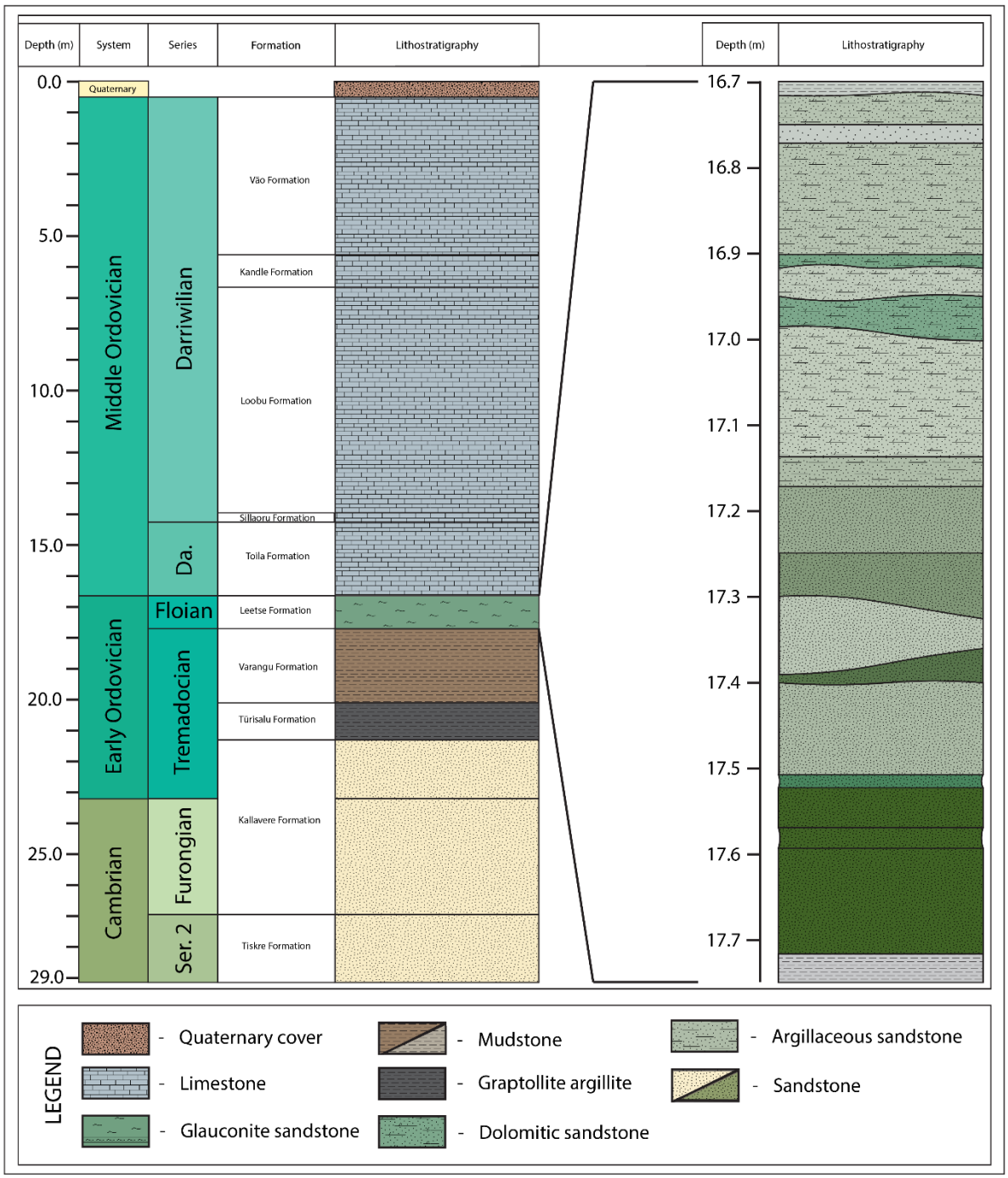

Figure 8. Lithostratigraphic column of the PH010B drillcore and detailed lithological description of the Leetse Formation. Modified after drillcore descriptions by Hints, O. from the e-Maapõu database; lithological subdivision created by the author.

5.2 SEM analysis of glauconite morphology and internal structures

5.2.1 External morphology

Across all analysed samples, glauconite predominantly occurs as discrete, rounded to sub-rounded

pellets. Grain sizes range from 80 to 500 µm and glauconite pellets are typically closely packed, forming grain-supported textures in the lower intervals and locally matrix supported textures in the upper part of the Leetse Formation (Figure 9).

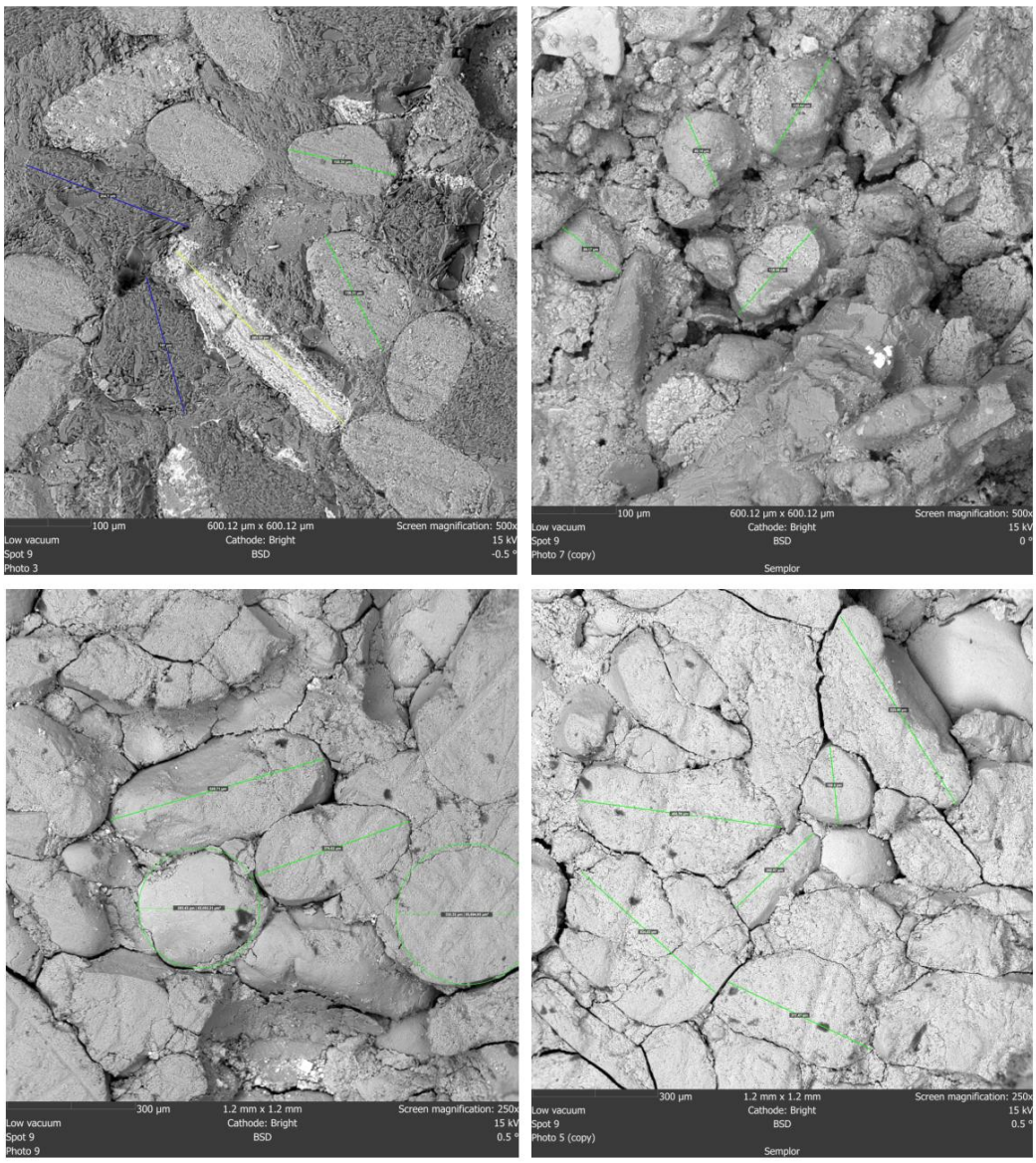

Figure 9. Morphological variability and size measurements of glauconite pellets observed under SEM-BSD imaging. (1) Subsample KBB25-002A (2) Subsample KBB25-010A (3) Subsample KBB25-016A (4) Subsample KBB25-018A.

The observable external structures of glauconite pellets ranged from relatively smooth and compact surfaces to rough and granular surfaces. Smooth glauconite pellets appear compact and homogeneous within the samples, with minor surface irregularities present. Contrarily, pellets with a granular surface can be characterized by fine particulate coatings and micro-aggregates adhering to pellet exteriors. In

some samples, pellets can be observed to display partial surface alteration, where smoother areas transition into more irregular, granular habits (Figure 10).

Localized cracking and micro-fracturing of grain surfaces can also be observed. In some cases, fractures appear to follow pre-existing structural weaknesses within the pellets. Some pellets additionally display slight surface deformation and compression features at grain contacts.

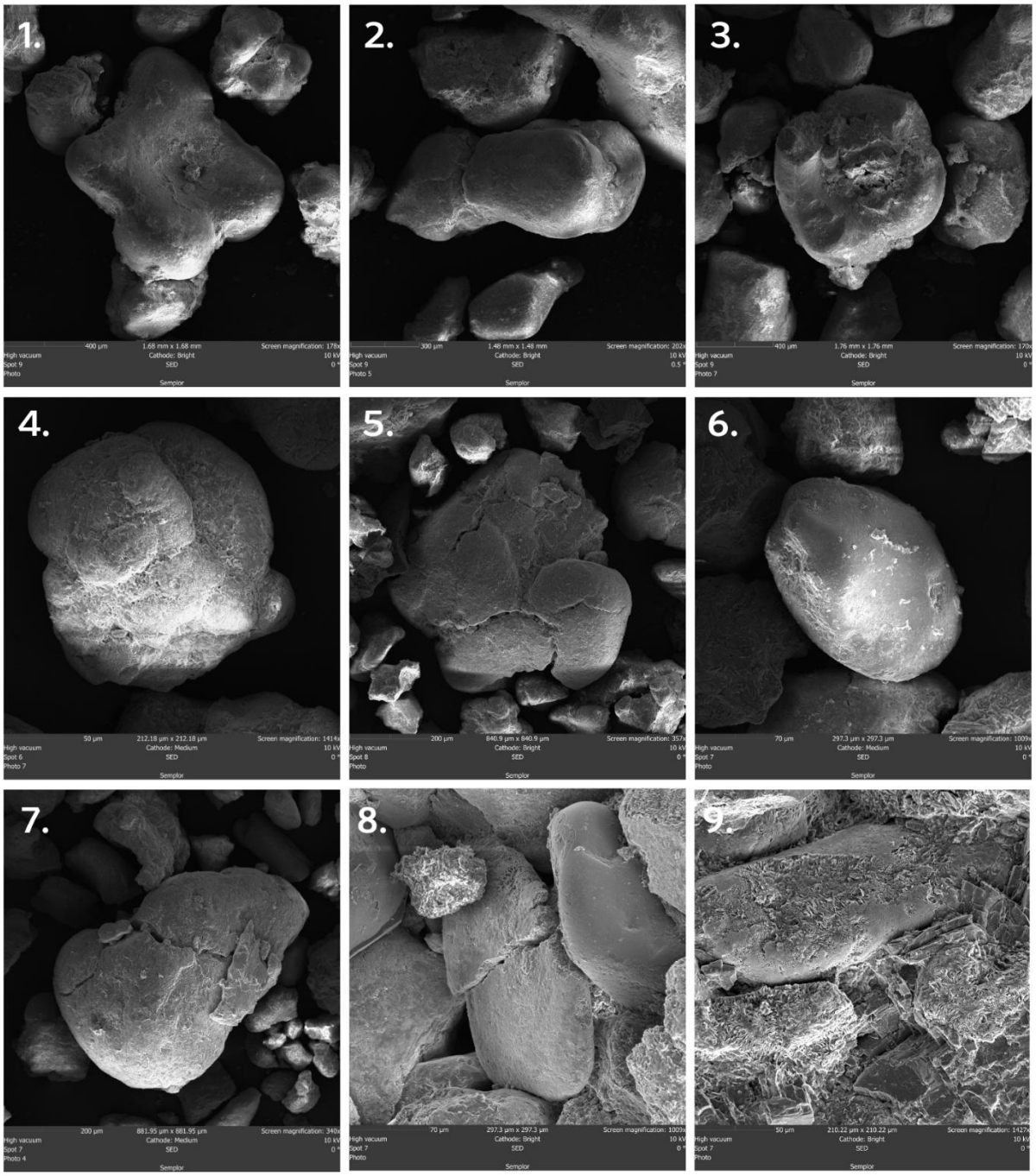

Figure 10. Morphological variability and surface characteristics of glaucontie observed under SEM-SED imaging. (1-3) Lower part of the Leetse Formation, subsamples KBB25-016/018 (4-5) Subsample KBB25-013A (6-7) Subsample KBB25-010A (8) Subsample KBB25-007A (9) Subsample KBB25-005A.

5.2.2 Internal structures of the pellets

Higher magnification observations of glauconite pellets reveal an internal composition of densely packed, fine fibrous to flaky microstructures, as shown in Figure 11. The internal build-up of the aggregates shows porous textures composed of interwoven lath-like crystallites, arranged in swirling or radiating, locally concentric, microscopic particles. More densely backed rims sometimes could be identified around more porous core of the pellets.

Several pellets display mechanical fragmentation and internal fracturing. Fractures can be mostly observed along grain boundaries and as internal cracks or voids, which sometimes divide pellets into sub-domains. In most fragmented pellets, the internal microstructure is exposed, which reveals the fibrous and layered nature of the glauconitic material. Despite some variability in surface characteristics across the depth interval, the internal microstructure of glauconite remains consistent defined by the previously described fibrous and lamellar arrangement.

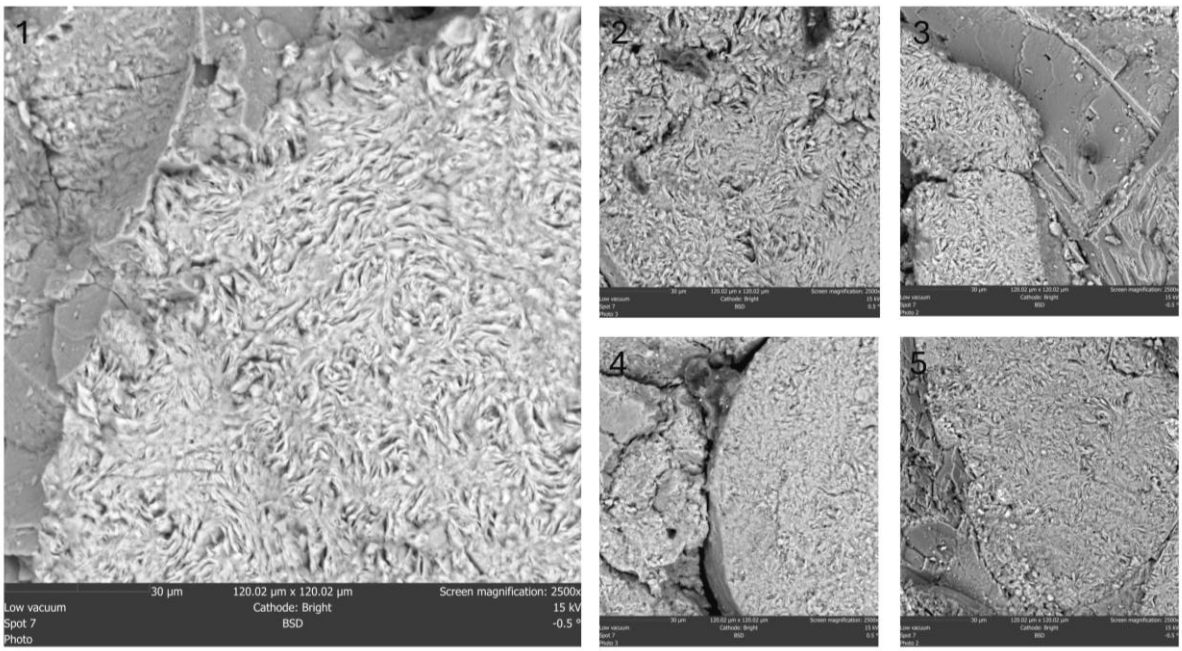

Figure 11. SEM-BSD images showing internal textures and microstructures of glauconite throughout the interval. (1) Subsample KBB25-007A: glauconite internal structure at grain border showing vermicular texture and swirling arrangement (2) Subsample KBB25-018A: compact flaky texture with microporosity (3) Subsample KBB25-005A: bordering glauconite grains (4) Subsample KBB25-016A: fine-grained compact internal structure at grain border (5) Subsample KBB25-002A: dense texture showing radiality and microporosity.

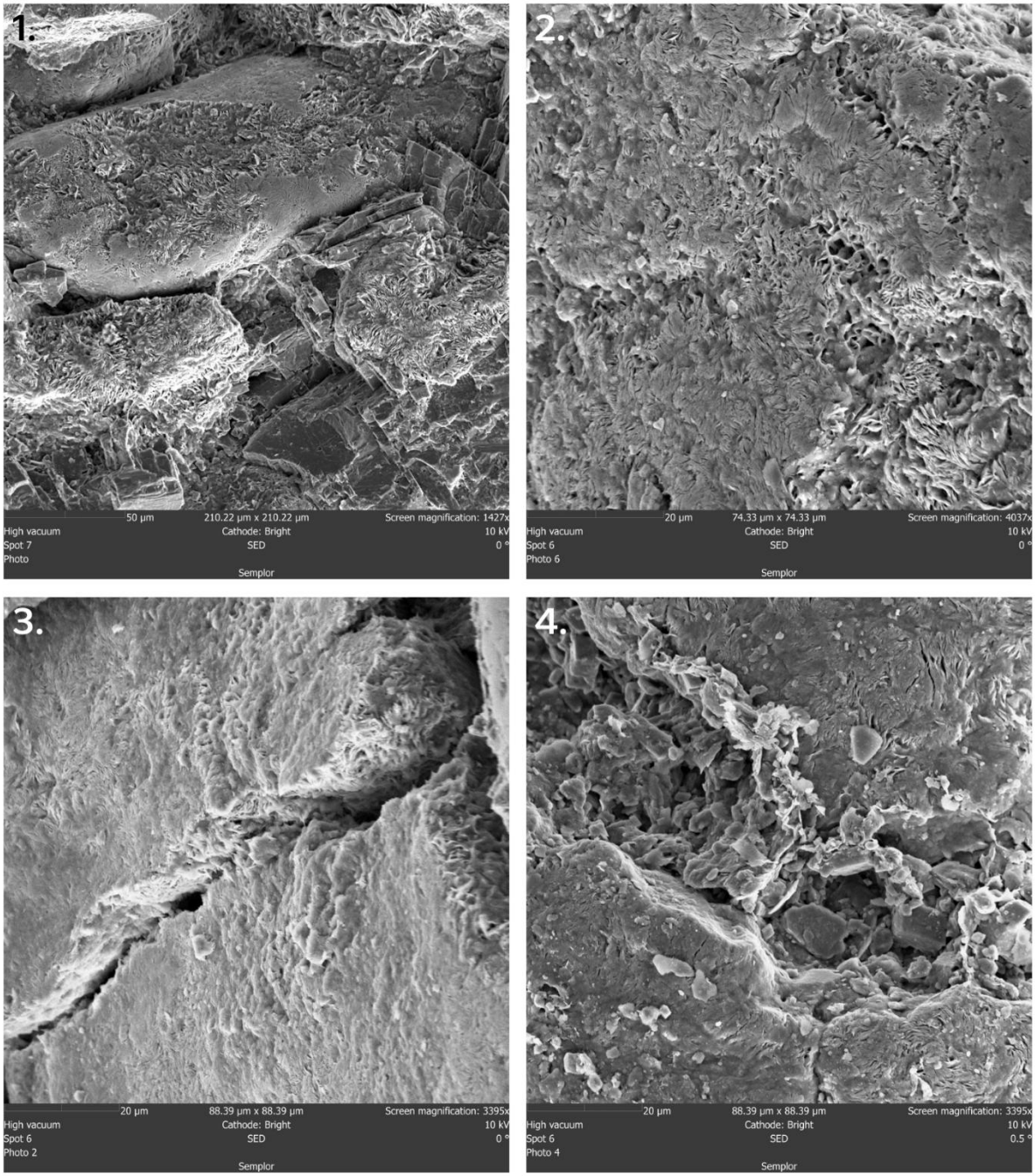

Figure 12. SEM-SED images showing internal textures and microstructures of glauconite throughout the interval. (1) Subsample KBB25-005A: smooth, partially spalled glauconite grain, revealing the flaky internal textures (2) Subsample KBB25-005A: honeycomb texture transition to flaky, radial textures in glauconite (3) Subsample KBB25-007A: crack in a glauconite grain, lamellar oriented crystallites (4) Subsample KBB25-013A: fragmented and collapsed flaky internal textures along cracks in glauconite grain.

5.2.3. Associated mineral phases and features

In addition to glauconite pellets within the samples, the analysed samples contain several associated mineral phases and sedimentary features that provide important context for interpreting the environment of the studied interval (Figures 13 and 14).

Angular to sub-angular detrital grains are present as interstitial material between glauconite pellets, particularly in the upper section of the interval. Energy dispersive spectroscopy (EDS) mapping of the upper interval (Figure 12, row 1) show that these grains are compositionally variable, with distinct areas enriched in Al, K, Mg and Ca. A bright elongate grain together with smaller, sub-angular grains visible in the BSD image of the same sample appear compositionally distinct with EDS indicating a phase enriched in P and Ca, suggesting phosphatic bioclast origin of the fragments.

Carbonate cement is locally abundant, especially in the upper sections of the studied interval. Cementation can be observed as pore-filling material surrounding glauconite pellets and detrital grains, forming irregular patches and locally reducing pore space. EDS mapping in the second row of Figure 12, row 2 shows carbonate dominated areas as elevated Ca and Mg signals in between and around glauconitic pellets.

The third row of Figure 12 shows a large, lobate grain, with EDS mapping identifying it as being enriched in Si and O internally, with Ti enriched coating, suggesting a terrigenous quartz grain coated by secondary phases, most likely anatase. The fourth row in the figure illustrates a well preserved rounded quartz grain with pronounced compositional variation. EDS mapping shows a core enriched in Si, with a distinct surrounding rim consisting of mainly Ca and P.

Figure 13 illustrates two additional associated features of interest. The left image shows a well-preserved conodont fossil fragment, surrounded by carbonate matrix and glauconite pellets. The two rightmost images capture massive aggregate of idiomorphic pyrite observed in the lower section of the studied interval.

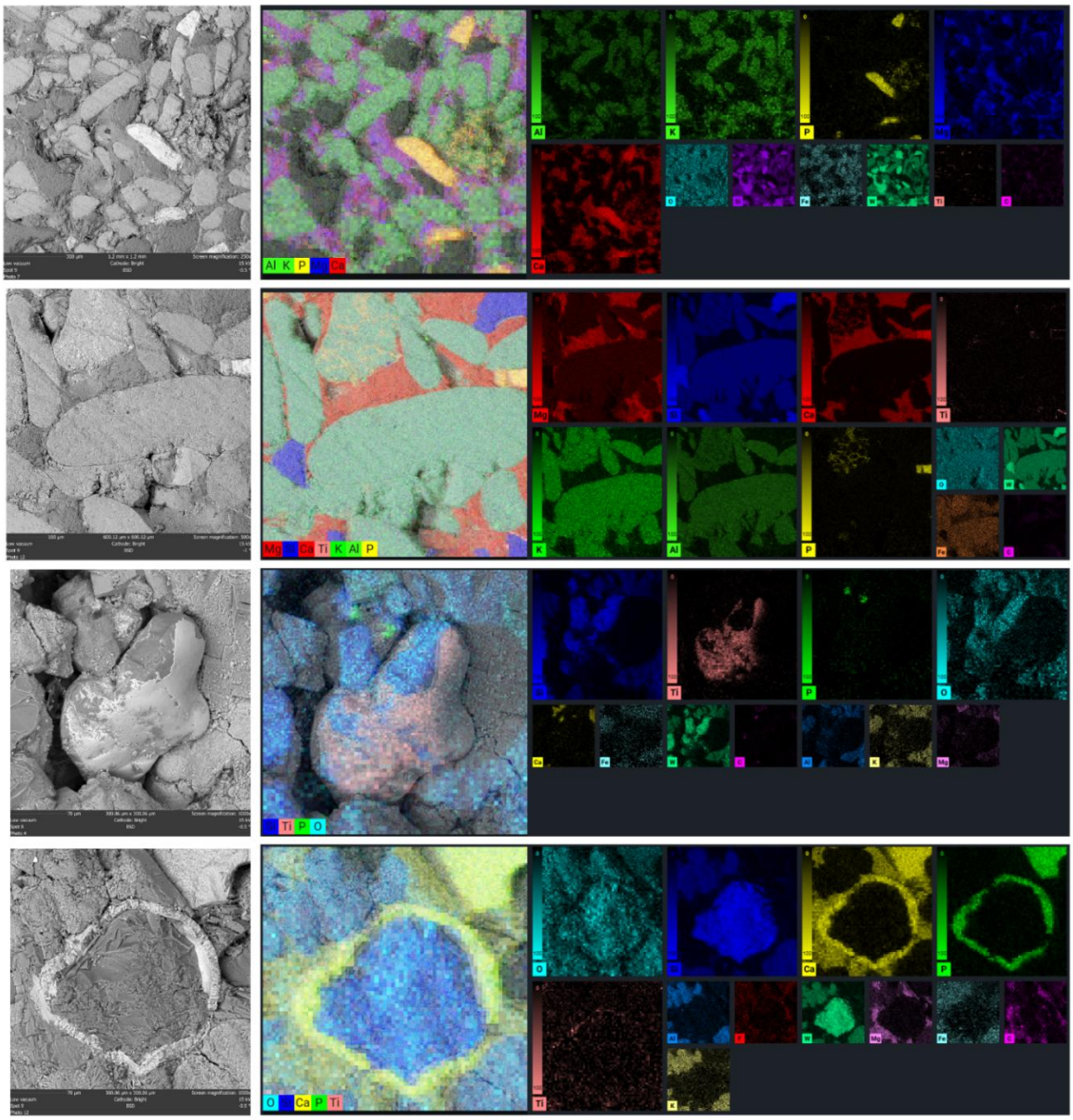

Figure 14. SEM-BDS images and corresponding EDS elemental maps.

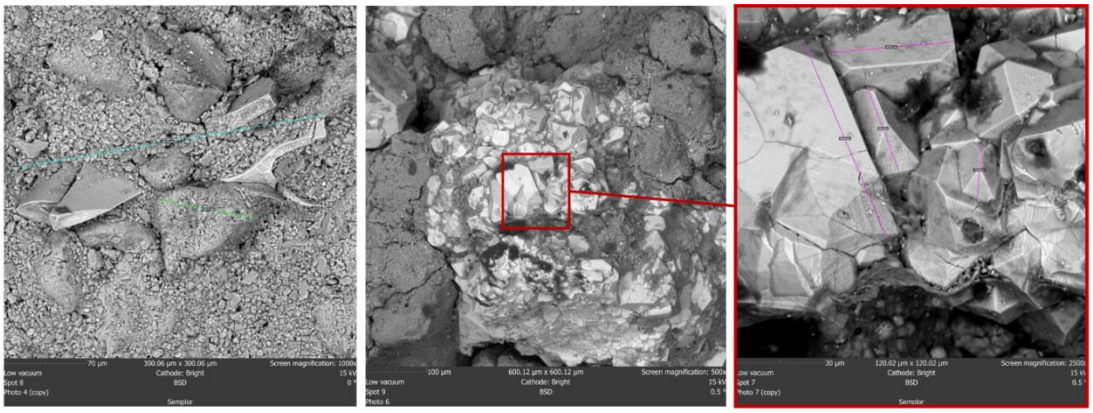

Figure 13. SEM-BSD images of associated features in drillcore PH010B. (Left) Conodont fossil fragment; (Centre and right) Pyrite aggregate.

5.3 XRD results and mineralogical composition

XRD analysis indicates glauconite being the dominant clay mineral phase throughout the analysed interval. The resulting diffraction patterns consistently show characteristic reflections attributable to glauconitic material, with variations in peaks intensity observed between samples. Semi-quantitative results show that glauconite contents range from 14.6% to 78.5%, with the majority of samples corresponding to lowermost part of the Leetse Formation, containing more than 50% glauconite (Figure 13). From other phyllosilicates, illite is present as a major phase throughout the Leetse Formation.

Other mineral phases in the studied section include quartz and carbonate phases, primarily dolomite. Quartz is present in all samples in moderate proportions. Dolomite occurrence varies notably. Higher dolomite concentrations appear in the upper part of the Leetse Formation where glauconite content is lower. Orthoclase, muscovite and apatite occur in low amounts across most samples. In several samples, the presence of additional clay minerals is indicated by weak diffraction patterns. Pyrite is detected in trace to minor amounts.

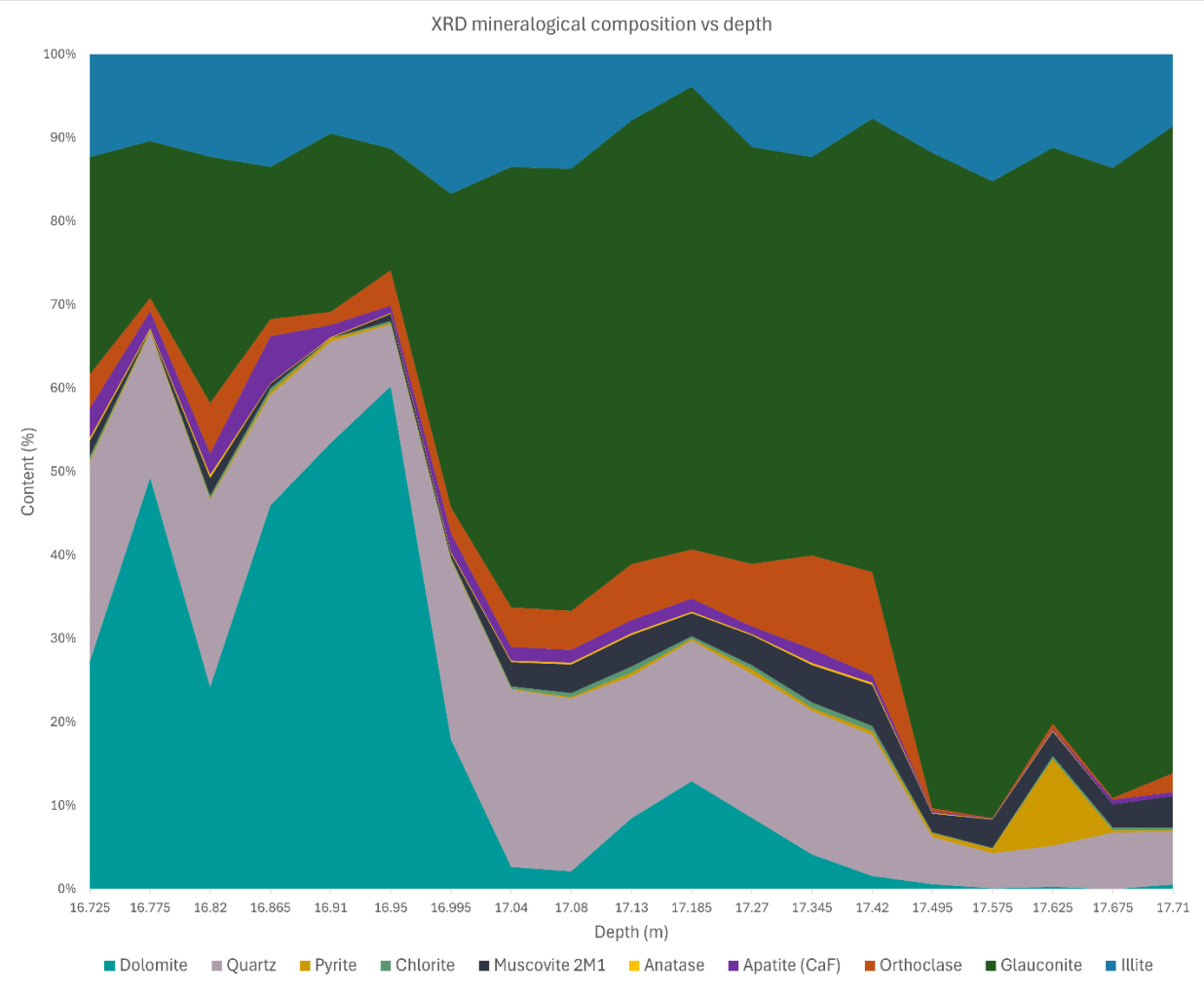

Figure 15. Downcore mineralogical composition of the studied glauconitic interval based on XRD.

5.4 XRF results and geochemical composition

5.4.1. Vertical geochemical variations

XRF analysis reveals systematic vertical variations in major element composition across the studied interval. The results are characterized by distinct changes in major element (K_2O, Fe_2O_3, Al_2O_3, SiO_2, and CaO) concentrations with depth (Figure 14).

In the upper part of the Leetse Formation (16.70-16.95 m), K_2O values are consistently low, generally below 3 wt%. This interval is characterized by relatively high SiO_2 contents, reaching up to 48 wt%, and elevated CaO concentrations, consistently exceeding 10 wt% and locally approaching 17 wt%. Fe_2O_3 values remain within a relatively narrow range of approximately 6.9 to 8.2 wt%, while Al_2O_3 concentrations vary between 4 and 8 wt%. Loss on ignition values are comparatively high in this interval reflective high content of carbonates.

Downsection, within the middle part of the interval (16.95–17.25 m), a pronounced increase in K_2O content is observed. Values rise sharply to between approximately 4 and 7 wt%, marking a clear transition relative to the overlying section. This increase is accompanied by elevated Fe_2O_3 concentrations, which ranges more widely and reach significantly higher values than in the upper interval in the lowermost part of the formation. Al_2O_3 concentrations remain moderate, generally between 6 and 12 wt%, while SiO_2 contents increases relative to the upper interval. CaO concentrations at the same time decline in comparison to the overlying samples.

In the lower section (17.25-17.72m), K_2O values remain consistently high, commonly exceeding 6 wt% and reaching up to approximately 7.8 wt%. Fe_2O_3 concentrations are also elevated, extending to approximately 25 wt%. Al_2O_3 shows moderate variability but remains within a similar range to that observed in the middle interval. SiO_2 contents are comparatively lower in the upper part of the section compared to the lower part, while reverse trend appears in case of CaO and MgO concentrations. In general geochemical variability between adjacent samples is less pronounced in the middle part of the Leetse Formation, resulting in a more uniform geochemical profile. Distinct compositional shift occurs near 17.42 depth, where Fe_2O_3 concentrations increase notably while SiO_2 decreases relative to the overlying interval. At the same time, Al_2O_3 contents also slightly decrease.

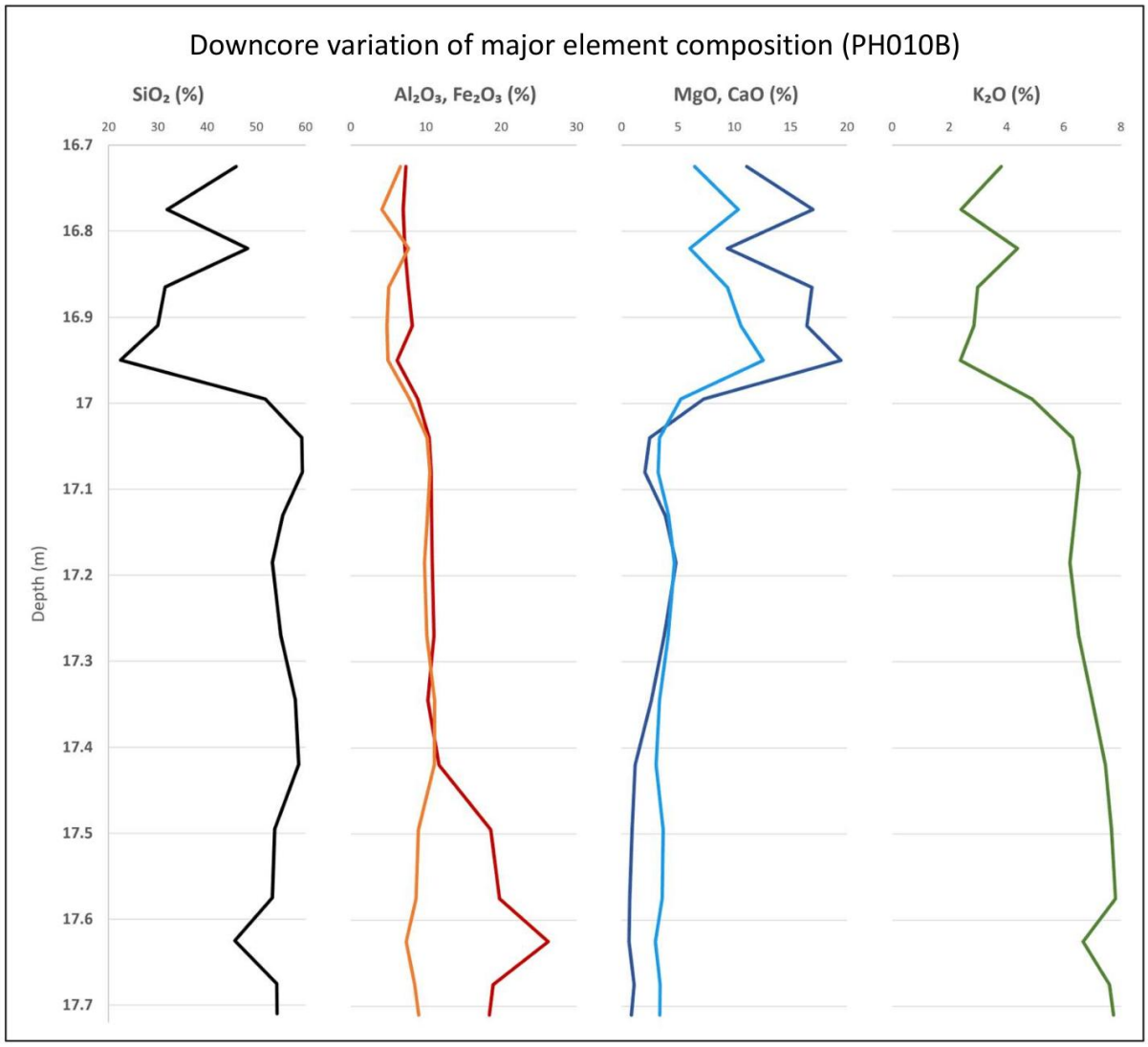

Figure 16. Downcore geochemical composition of major elements based on XRF analysis.

5.4.2. Major element relationships

The bivariate relationships between major elements reveal several significant trends that reflect the varying glauconite content and mineralogical mixing between glauconitic, siliciclastic and carbonate components across the studied interval (Figure 17).

The relationship between K_2O and Fe_2O_3 represents a positive but more scattered trend (R^2=0.51), indicating moderately strong correlation. Several samples deviate notably from the regression line, most notably, a group of samples clusters at moderate K_2O values of approximately 6-7 wt% but shows a wide range of Fe_2O_3 concentrations, from around 9 to 26 wt%.

K_2O and CaO display a very strong negative correlation (R^2=0.96). High CaO concentrations correspond consistently to low K_2O values and the trend is well defined across the full compositional range of the samples.

The relationship between K_2O and Al_2O_3 shows positive relatively strong correlation (R^2=0.72). Although progressive increase of K_2O is consistent with an increase of Al_2O_3, with a clear clustering of low-K_2O/low-Al_2O_3 samples and high-K_2O/high-Al_2O_3 samples, minor scattering occurs throughout the dataset.

K_2O and SiO_2 exhibit strong positive correlation (R^2=0.76). Although several samples with elevated K_2O contents also display moderate to high SiO_2 concentrations, the dataset shows greater scatter and does not form a single strongly constrained linear trend.

The relationship between SiO_2 and Al_2O_3 displays very strong positive correlation (R^2=0.88). Al_2O_3 increases with increasing SiO_2, forming a well-defined trend across the dataset. In contrast, the Al_2O_3 and Fe_2O_3 shows no clear correlation (R^2=0.08), with no systematic trend emerging.

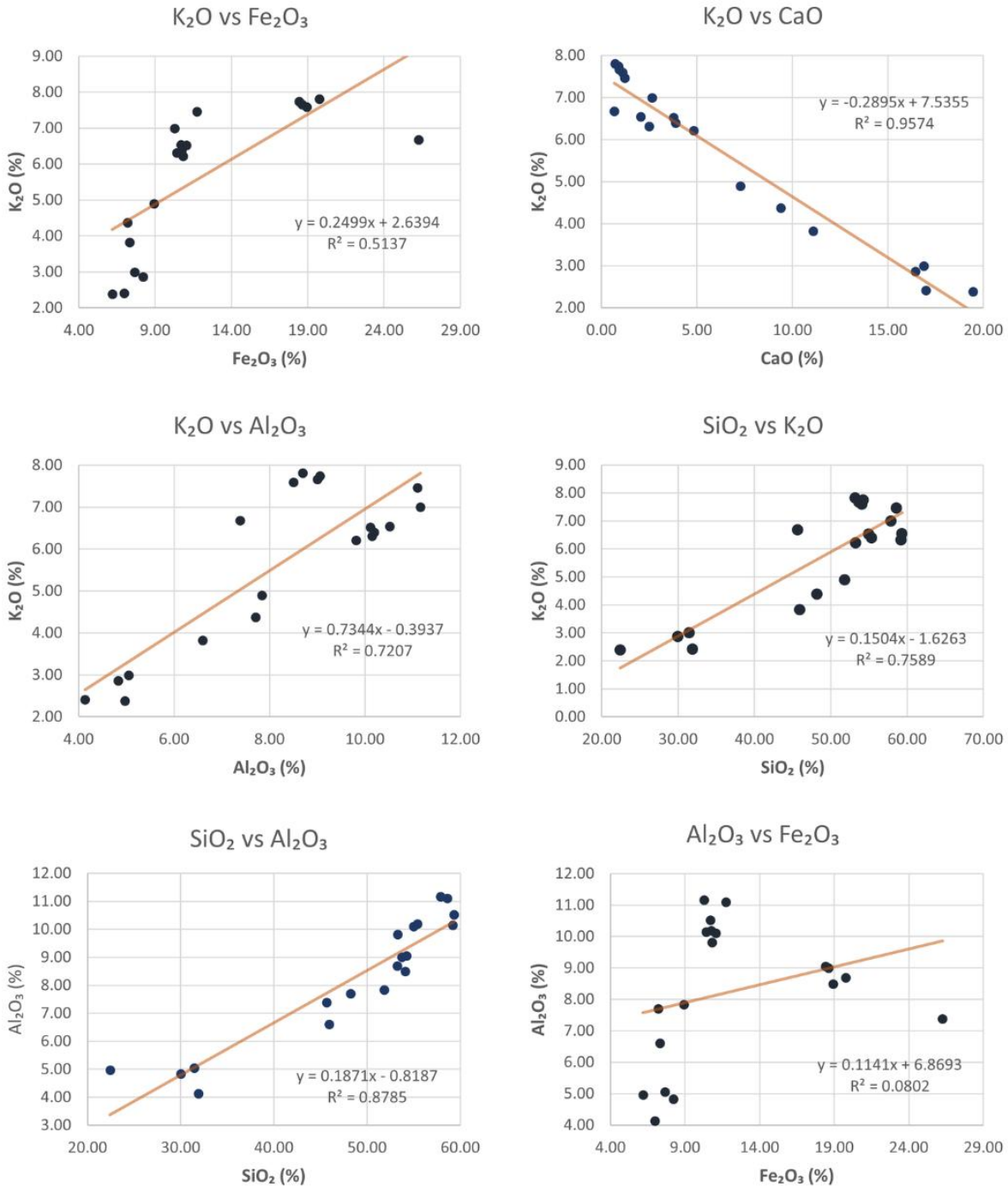

Figure 17. Bivariate relationships between major elements derived from XRF analysis of glauconitic samples.

5.5 Integrated observations

The combined observations and datasets from macroscopical, microscopical and geochemical datasets demonstrate a systematic vertical transition within the studied interval from carbonate- and quartz-rich glauconitic sandstone in the upper section towards increasingly glauconite-dominated phases downcore. SEM observations reveal that glauconite occurs predominantly as rounded to sub-rounded pellets with fibrous and lamellar internal textures, consistent throughout the interval. The

mineralogical trends identified by XRD closely correspond to geochemical patterns observed in XRF datasets. Intervals with elevated glauconite abundances are characterized by increased K_2O and Fe_2O_3 concentrations, while carbonate-rich intervals display elevated CaO contents and lower glauconite concentrations. Overall, the integrated dataset indicates that glauconite distribution, mineralogical composition and geochemical characteristics are closely related to lithological variability.

6. Discussion

6.1 Morphological characteristics

Microanalysis of representative samples and corresponding glauconite from drillcore PH010B reveals morphological features consistent with authigenic formation in a shallow marine shelf environment. The predominance of rounded to sub-rounded pellets corresponds well with previous descriptions of authigenic glauconite peloids reported from Lower Ordovician shelf deposits and other glauconitic marine successions (Burst, 1958; Krainer 2022). The generally good rounding of pellets suggests weak and repeated reworking and extended residence near the sediment-water interface, where prolonged interaction with seawater was a facilitator of the glauconitisation process.

The variation in external pellet morphology, ranging from smooth to rough and granular surfaces, is a likely reflection of differences in pellet evolution, surface alteration and local diagenetic modification. Smooth and homogeneous pellets are associated with more advanced stages of glauconitisation, while irregular textures may indicate incomplete mineral transformation or secondary alteration processes (Krinsley, 1998; Thompson, 1975). Transitional surface textures observed throughout individual grains additionally suggest that glauconitisation did not occur uniformly throughout the studied interval.

SEM observations of the internal structures of the aggregates demonstrate that the glauconite pellets in the upper part of the Leetse Formation are composed of flaky and porous textures. Downward, the textures evolve to more fibrous-lamellar microstructures consisting of densely packed lath-like crystallites. Similar internal structures have been described in modern and historical glauconitic grains and are considered a characteristic of authigenic glauconite formed through progressive transformation of Fe-rich clay precursors during early diagenesis (Lopez-Quiros, 2020). The occurrence of porous and heterogenous internal flaky textures in the upper interval of the Leetse Formation suggests incomplete compaction and preservation of early diagenetic textures, while the denser and more lamellar microstructures in the lower intervals reflect a more advanced stage of mineralogical development.

Fracturing and localized cracking are common throughout the analysed interval and occur primarily along pellet margins and internal textural boundaries. These observed features likely reflect post-depositional compaction and deformation during burial. Despite variability in external morphology and surface alteration, the persistence of common internal textures throughout the interval suggests relatively consistent authigenic mineralogical development of glauconite.

The microscopical observations of glauconite support the interpretation that the pellets likely originated as fecal pellets. Rounded morphologies, internal heterogeneity and localized internal cavities resemble structures often associated with biologically mediated glauconitisation described in previous studies (Tribovillard, 2023). Although biological precursor structures are not always preserved, the morphology of the pellets strongly indicates an authigenic origin linked to early diagenetic processes within organic-rich microenvironments, most plausibly within fecal pellet substrates.

6.2 Maturity and evolution of glauconite

The mineralogical and geochemical dataset shows a clear variation in glauconite evolution within the studied interval. The systematic increase in K_2O and Fe_2O_3 concentrations downcore, together with increasing glauconite abundance identified through XRD analysis, provides the primary evidence for this trend.

The upper part of the studied interval is characterized by comparatively low K_2O concentrations, elevated CaO contents and increased carbonate cementation. This is combined with observed lower glauconite abundance and a less evolved stage of glauconitisation. Contrastingly, the lower part of the interval shows higher K_2O values, together with elevated Fe_2O_3 and higher proportions of glauconite identified by XRD. According to the widely applied glauconite maturity classifications, increasing potassium content reflects progressive incorporation of K^+ into interlayer sites and increasing structural ordering of glauconitic minerals (Thompson, 1975; Rafiei, 2023). 2

The downcore evolution of glauconite is reflected well in geochemical ratios. The K/Al and Fe/Al ratios increase towards the base of the studied interval, suggesting that the glauconite in the lower sections of the Leetse Formation is not only more abundant but also compositionally distinct. A particularly clear geochemical boundary is apparent around the depth 17.42 m. Below this boundary, Fe_2O_3 is markedly elevated relative to both K_2O and Al_2O_3, suggesting that the glauconite in the lowermost part of the Leetse Formation is notably iron-rich by comparison with the overlying glauconitic intervals. The ratios of Fe/Al combined with moderately elevated K_2O below the boundary may indicate an early or intermediate stage of glauconitisation characterised by strong iron incorporation but less complete potassium uptake, consistent with glauconite forming under sustained suboxic to mildly reducing conditions at or near the sediment-water interface (Tribovillard, 2024).

The colour of glauconite pellets also supports a maturity gradient in the Leetse Formation. Pellets from the lower part of the formation appear darker green, consistent with higher iron and potassium contents characterising more evolved glauconite, while pellets in the upper interval take on more yellow-green hues associated with less mature, Fe-smectite rich precursor phases.

6.3 Glauconite genesis in the Toolse drillcore

The combined analyses of drillcore PH010 support the theory of predominantly authigenic in situ glauconite formation within the Toolse deposit, with fecal pellets as the likely dominant precursor substrate. The rounded to sub-rounded morphology, fibrous internal microstructures and widespread distribution of glauconite pellets throughout the interval are all consistent with glauconitisation initiated within organic-rich microenvironments, conditions most commonly created by the decomposition of fecal pellets at or near the sediment-water interface (Tribovillard, 2023; Lopez-Quiros, 2020). These findings and interpretations place the Toolse deposit glauconite within the established model of marine shelf glauconitisation, where biological substrates provide both the structural framework and the localised reducing environments required for iron incorporation and clay transformation.

The occurrence of pyrite in trace amounts in the Leetse Formation further supports the presence of reducing conditions during early digenesis. Pyrite precipitation is often associated with organic matter degradation and reducing pore-water environments, conditions which also favour the coexistence of Fe^{2+} and Fe^{3+} required for glauconitisation (Tribovillard, 2024). Despite the overall high iron content of the glauconitic sandstone, pyrite contents remain negligible throughout the interval, which indicates that the majority of iron was partitioned into glauconite rather than into sulphide phases, implying that conditions were reducing enough to reduce iron but not sufficiently reducing to drive notable sulphate reduction.

Although the majority of glauconite appears authigenic, evidence for limited sedimentary reworking cannot be excluded. The generally rounded pellet morphologies and moderate sorting indicates that minor transport and redistribution of glauconite grains may have occurred within the depositional basin. However, the preservation of internal microstructures and the absence of extensive surface abrasion show that transport distances were likely limited.

The vertical increase in glauconite abundance and maturity downcore may reflect periods of particularly low sedimentation and sediment starvation, conditions commonly associated with condensed marine shelf deposits and transgressive systems (Banerjee, 2016). Under such conditions, sediment particles remain exposed at the sediment-water interface for extended periods, allowing progressive potassium uptake and mineralization. The distinct geochemical transition at 17.42 m may illustrate an episode of intensified glauconitisation or a change in depositional dynamics at that level, possibly linked to a shift in sedimentation rates or a transient change in pore-water chemistry. Below this boundary, the iron-rich glauconite may reflect sustained suboxic conditions and enhanced iron availability during the earliest stages of Leetse Formation deposition in this part of the Toolse area.

Combined, the findings from drillcore PH010B establish several novel findings for the Toolse deposit and the Estonian Leetse Formation. Direct microstructural evidence for fecal pellet precursors, a documented downcore microstructural maturity gradient, the identification of a geochemical boundary with iron-rich glauconite below it, and a redox reconstruction based on the iron-pyrite balance that indicates glauconitisation firmly within suboxic microenvironmental conditions. These findings refine the understanding of glauconite genesis in the Early Ordovician Baltic Palaeobasin and provide a basis for more targeted future investigations of maturity and resource potential within Estonian glauconite deposits.

6.4 Limitations

Several limitations should be taken into consideration when interpreting the results of this study. The study and analysis is based on a single drillcore, which limits the ability to assess the lateral variability of glauconite across the Toolse deposit. Although vertical trends are well documented and constrained, projection to the broader depositional system of the area requires a conservative approach.

The mineral interpretations are constrained by the resolution of bulk XRD analysis. Certain minor clay mineral phases may remain unresolved due to overlapping diffraction peaks and the complex mixed-layer nature of glauconitic material. More detailed clay mineral characterization, including oriented

clay preparations or transmission electron microscopy, could provide additional insight into the structural evolution of glauconite. SEM observations are based on a limited number of representative samples and therefore may not fully capture the entire morphological variability present throughout the interval. Some observed textures and fracture patterns may also reflect sample preparation effects or traces of polishing. The geochemical dataset mostly focuses on major element distributions, while trace element and isotopic analyses remained beyond the scope of the present study. Such analyses could further constrain redox conditions, sediment provenance and diagenetic evolution within the depositional system.

7. Author's contributions

The author of this study contributed to drillcore preparation, description and sawing; conducted high-resolution drillcore scanning; prepared XRF pellet samples; prepared and analysed SEM epoxy mounts; and prepared SEM gain mounts for gold coating a subsequent SEM laboratory analysis.

8. Acknowledgements

Finally, I would like to give my warmest thanks to several individuals from the Department of Geology, who played key roles in the completion of this thesis.

An immense thank you to my supervisor, Rutt Hints, whose expertise, support and scientific approach helped me develop my research and build a better understanding of the subject. I also extend my gratitude to the XRF/XRD laboratory team – Toivo Kallaste, Nata-Ly Pantšenko and Erki Leht – who played instrumental roles in sample preparation and data analysis. I am equally grateful to Olle Hints, Gennadi Baranov, Siim Roov, Sophie Graul and Carina Sula for their support, time and expertise, each of which contributed to different aspects of this work.

References

Anso, J. (1947). *Glaukoniit kaalisoola allikana*. RK "Teaduslik Kirjandus".

Banerjee, S., Bansal, U., & Thorat, A. V. (2016). A review on palaeogeographic implications and temporal variation in glaucony composition. *Journal of Palaeogeography, 5*(1), 43–71. https://doi.org/10.1016/j.jop.2015.12.001

Bauert, H., Soesoo, A., & Hade, S. (eds). (2015). Strategic raw materials of Estonia. In *Strategic raw materials of Estonia* (pp. 1–55).

Brouwer, P. (2010). *Theory of XRF: Getting acquainted with the principles* (3rd ed.). PANalytical B.V.

Burst, J. F. (1958). "Glauconite" pellets: Their mineral nature and applications to stratigraphic interpretations. *AAPG Bulletin, 42*(2), 310–327.

Chafetz, H. S., & Reid, A. (2000). Syndepositional shallow-water precipitation of glauconitic minerals. *Sedimentary Geology, 136*, 29–42.

Edward, O., Korte, C., Ullmann, C. V., Colmenar, J., Thibault, N., Bagnoli, G., Stouge, S., & Rasmussen, C. M. Ø. (2022). *A Baltic perspective on the Early to early Late Ordovician δ13C and δ18O records and its paleoenvironmental significance*. *Paleoceanography and Paleoclimatology, 37*(3), e2021PA004309. https://doi.org/10.1029/2021PA004309

El-Habaak, G., & Abdel-Hakeem, M. (2023). Potential exploitation of the Phanerozoic glauconites in Egypt. In Z. Hamimi et al. (Eds.), *The Phanerozoic geology and natural resources of Egypt* (Advances in Science, Technology & Innovation). Springer. https://doi.org/10.1007/978-3-030-95637-0_19

Ermrich, M., & Opper, D. (2013). *X-ray powder diffraction: XRD for the analyst* (2nd rev. ed.). PANalytical B.V.

Grundmann, G., & Scholz, H. (2015). *The preparation of thin sections, polished sections, acetate foil prints, preparation for elutriation analysis, and staining tests for the optical and electron microscopy*. Technische Universität München.

Heinsalu, H. N. (1970). *Глауконитовые песчаники Эстонской ССР и возможности их использования* [Glauconitic sandstones of the Estonian SSR and their potential uses]. Geological Survey of the Estonian SSR.

Heinsalu, H., Viira, V., & Raudsep, R. (1994). Environmental conditions of shelly phosphorite accumulation in the Rakvere phosphorite region, northern Estonia. *Proceedings of the Estonian Academy of Sciences, Geology, 43*(3), 109–121.

Hower, J. (1961). Some factors concerning the nature and origin of glauconite. *American Mineralogist, 46*, 313–334.

Huggett, J. (2005). Glauconites. In *Encyclopedia of Geology* (Vol. 3, pp. 542–548). Elsevier.

Ivanovskaya, T. A., Sakharova, B. A., & Zaitsev, T. S. (2023). Globular phyllosilicates of the glauconite–illite series in the Cambrian and Ordovician rocks of the Eastern Baltica. *Lithology and Mineral Resources, 58*(2), 158–176.

Kannan, M. (n.d.). *Scanning electron microscopy: Principle, components and applications*. In *A textbook on fundamentals and applications of nanotechnology* (pp. 81–84). Astral International.

Kirs, J., Puura, V., Soesoo, A., Klein, V., Konsa, M., Koppelmaa, H., Niin, M., & Urtson, K. (2009). *The crystalline basement of Estonia: Rock complexes of the Palaeoproterozoic Orosirian and Statherian and Mesoproterozoic Calymmian periods, and regional correlations*. *Estonian Journal of Earth Sciences, 58*(4), 219–228. https://doi.org/10.3176/earth.2009.4.01

Krainer, K., Tropper, P., Krenn, K., & Lucas, S. G. (2022). Occurrence and origin of glauconite in the Cambro–Ordovician Bliss Formation of southern New Mexico and West Texas (USA). *Journal of Sedimentary Research, 92*, 353–370.

Krinsley, D. H., Pye, K., Boggs, Jr, S., & Tovey, N. K. (1998). Glauconite. In *Backscattered Scanning Electron Microscopy and Image Analysis of Sediments and Sedimentary Rocks* (pp. 131–144). chapter, Cambridge: Cambridge University Press.

Lee, Y. I., & Paik, I. S. (1997). High alumina glaucony from the Early Ordovician Mungok Formation, Korea. *Geoscience Journal, 1*(2), 108–114.

López-Quirós, A., Sánchez-Navas, A., Nieto, F., & Escutia, C. (2020). New insights into the nature of glauconite. *American Mineralogist, 105*, 674–686. https://doi.org/10.2138/am-2020-7341

Nestor, H., Soesoo, A., Linna, A., Hints, O., & Nõlvak, J. (2006). *Ordoviitsium Eestis ja Lõuna-Soomes* [The Ordovician in Estonia and South Finland]. GEOGuide Baltoscandia.

Pandey, S., Mishra, S., Sardar, T., Khan, A., Parmar, B., & Mishra, A. (2025). Sample preparation techniques for scanning electron microscopy. *Integrated Ferroelectrics, 241*(7–9), 732–744. https://doi.org/10.1080/10584587.2025.2483653

Penny, A. M., Hints, O., & Kröger, B. (2021). *Carbonate shelf development and early Palaeozoic benthic diversity in Baltica: A hierarchical diversity partitioning approach using brachiopod data*. *Paleobiology, 47*(3), 1–21. https://doi.org/10.1017/pab.2021.3

Pihel, R. (2025). *Mehhaaniliselt aktiveeritud Eesti glaukoniitliivakivi kaaliumväetise toormena* [Mechanically activated Estonian glauconitic sandstone as a raw material for potassium fertilizer] (Master's thesis, University of Tartu).

Puura, V. (Ed.). (1987). *Geology and mineral resources of the Rakvere phosphorite-bearing area*. Valgus Publishers.

Rafiei, M., Löhr, S. C., Alard, O., Baldermann, A., Farkaš, J., & Brock, G. A. (2023). Microscale petrographic, trace element, and isotopic constraints on glauconite diagenesis in altered sedimentary sequences: Implications for glauconite geochronology. *Geochemistry, Geophysics, Geosystems, 24*, e2022GC010795. https://doi.org/10.1029/2022GC010795

Raukas, A., Teedumäe, A. (eds). 1997. Geology and Mineral Resources of Estonia. Estonian Academy Publishers, Tallinn. 436 pp.

Spoljaric, N. & Crawford, W.A. (1978) Glauconitic greensand: A possible filter of heavy metal cations from polluted waters. *Geo* 2, 215–221. https://doi.org/10.1007/BF02380487

Teedumäe, A. (1990). Lubjakivid Toolse fosforiidimaardlas [Limestones in the Toolse phosphorite deposit]. *Proceedings of the Estonian Academy of Sciences, Geology, 39*(1), 33–38.

Thompson, G. R., & Hower, J. (1975). The mineralogy of glauconite. *Clays and Clay Minerals, 23*, 289–300.

Tiyana, R. A., Supriyanto, Astuti, T. R. P., Jabbar, G. A., & Septyandy, M. R. (2022). Mineralogy, geochemistry, and genesis of glauconite mineral from paleotsunami deposit in Lebak, Banten, Indonesia. *E3S Web of Conferences, 340*, 01004. https://doi.org/10.1051/e3sconf/202234001004

Tribovillard, N. (2024). Revisiting shallow glauconite factories: Intertwined fates of glauconite and iron. *Comptes Rendus Géoscience, 356*, 139–155. https://doi.org/10.5802/crgeos.274

Tribovillard, N., Bout-Roumazeilles, V., Abraham, R., Ventalon, S., Delattre, M., & Baudin, F. (2022). The contrasting origins of glauconite in the shallow marine environment highlight this mineral as a marker of paleoenvironmental conditions. *Comptes Rendus Géoscience, 355*, 213–228. https://doi.org/10.5802/crgeos.170

Triplehorn, D. M. (1966). Morphology, internal structure, and origin of glauconite pellets. *Sedimentology, 6*(4), 247–266. https://doi.org/10.1111/j.1365-3091.1966.tb01503.x

Viira, V., Mens, K., & Nemliher, J. (2006). *Lower Ordovician Leetse Formation in the North Estonian Klint area*. Proceedings of the Estonian Academy of Sciences, Geology, 55(2), 156–174. https://doi.org/10.3176/geol.2006.2.05

Appendices

Appendix 1. XRD analysis raw results

XRD poolkvantitatiivne Rietveldi meetod

Mineraalide sisalduste (%) arvutamisel kasutati võrdluseks puhast kvartsi ja XRF tulemustest arvutatud neeldumiskoefitsente (mass attenuation coefficient)

	KBB-001	KBB-002	KBB-003	KBB-004	KBB-005	KBB-006	KBB-007	KBB-008	KBB-009	KBB-010	KBB-011	KBB-012	KBB-013	KBB-014	KBB-015	KBB-016	KBB-017	KBB-018	KBB-019
Dolomite	27.3	49.2	24.2	46.0	53.4	60.2	17.9	2.6	2.1	8.5	12.9	8.6	4.2	1.6	0.6	0.1	0.3	0.0	0.6
Quartz	23.9	17.4	22.4	13.2	12.2	7.4	21.5	21.3	20.7	17.0	16.9	17.2	17.2	16.9	5.6	4.2	4.9	6.8	6.3
Pyrite	0.21	0.25	0.19	0.38	0.36	0.19	0.15	0.10	0.18	0.45	0.23	0.53	0.36	0.44	0.44	0.56	10.40	0.29	0.14
Chlorite	0.5	0.1	0.3	0.5	0.0	0.3	0.2	0.3	0.5	0.7	0.3	0.5	0.7	0.6	0.1	0.1	0.3	0.3	0.4
Muscovite 2M1	1.8	0.0	2.1	0.5	0.0	0.8	0.5	2.9	3.4	3.8	2.8	3.6	4.5	4.9	2.2	3.4	2.9	2.8	3.7
Anatase	0.35	0.17	0.40	0.07	0.11	0.09	0.19	0.18	0.21	0.21	0.17	0.13	0.25	0.23	0.08	0.08	0.13	0.01	0.01
Apatite-(CaF)	3.6	2.1	2.5	5.6	1.5	0.9	2.2	1.6	1.5	1.6	1.6	0.9	1.7	0.9	0.2	0.1	0.2	0.6	0.5
Orthoclase	4.1	1.6	6.0	2.1	1.6	4.2	3.1	4.7	4.7	6.7	5.9	7.5	11.2	12.3	0.4	0.0	0.6	0.2	2.3
Glauconite	26.0	18.8	29.5	18.2	21.4	14.6	37.6	52.8	53.0	53.2	55.4	49.9	47.7	54.3	78.5	76.2	69.0	75.5	77.5
SUM	**87.7**	**89.6**	**87.7**	**86.5**	**90.5**	**88.7**	**83.3**	**86.5**	**86.3**	**92.1**	**96.1**	**88.9**	**87.7**	**92.3**	**88.2**	**84.8**	**88.8**	**86.4**	**91.4**
arvutuslik illiit	12.3	10.4	12.3	13.5	9.5	11.3	16.7	13.5	13.7	7.9	3.9	11.1	12.3	7.7	11.8	15.2	11.2	13.6	8.6
alla avastamispiiri																			

XRD analüüsi kontrolliks XRF tulemustest arvutatud dolomiidi ja püriidi sisaldused

Dolomite_XRF	26.8	49.5	24.0	43.2	50.1	61.7	16.6	3.1	2.1	7.9	11.2	8.1	3.7	1.3	1.5	0.9	1.1	1.2	1.1
Pyrite_XRF	0.20	0.33	0.21	0.43	0.43	0.31	0.16	0.09	0.15	0.28	0.23	0.33	0.32	0.33	0.27	0.34	14.97	0.15	0.22

Võreparameetrid

Glauconite_b, Å	9.055	9.041	9.038	9.047	9.051	9.032	9.046	9.045	9.048	9.049	9.053	9.053	9.051	9.056	9.065	9.067	9.070	9.067	9.068
Dolomite_a, Å	4.8152	4.8153	4.8148	4.8157	4.8158	4.8154	4.8157			4.8162	4.8165	4.8165							
Dolomite_c, Å	16.0643	16.0649	16.0663	16.0646	16.0640	16.0632	16.0645			16.0668	16.0655	16.0669							

Appendix 2. XRD fusion analysis raw results

XRF sulatus

Sample	LOI950°C	SiO2 (%)	TiO2 (%)	Al2O3 (%)	Fe2O3 (%)	MnO (%)	MgO (%)	CaO (%)	Na2O (%)	K2O (%)	P2O5 (%)	S (%)
KBB-001	15.01	45.93	0.55	6.60	7.31	0.17	6.48	11.09	0.08	3.82	1.86	**0.11**
KBB-002	24.75	31.92	0.35	4.13	6.97	0.29	10.34	16.99	0.04	2.41	1.19	**0.18**
KBB-003	13.65	48.22	0.56	7.70	7.19	0.15	6.06	9.40	0.05	4.38	1.33	**0.11**
KBB-004	22.35	31.45	0.27	5.05	7.66	0.25	9.38	16.89	0.07	2.99	2.36	**0.23**
KBB-005	25.06	30.00	0.22	4.83	8.21	0.30	10.59	16.44	0.06	2.86	0.72	**0.23**
KBB-006	30.26	22.41	0.26	4.96	6.18	0.36	12.57	19.46	0.07	2.38	0.36	**0.17**
KBB-007	10.81	51.81	0.38	7.84	8.93	0.10	5.25	7.28	0.06	4.89	1.41	**0.08**
KBB-008	5.10	59.19	0.36	10.15	10.41	0.02	3.35	2.48	0.08	6.31	0.99	**0.05**
KBB-009	4.78	59.33	0.38	10.52	10.70	0.02	3.25	2.06	0.08	6.54	0.90	**0.08**
KBB-010	7.15	55.37	0.34	10.19	10.74	0.05	4.17	3.87	0.07	6.40	0.94	**0.15**
KBB-011	8.55	53.25	0.31	9.81	10.81	0.07	4.68	4.82	0.05	6.21	0.90	**0.13**
KBB-012	7.23	54.99	0.34	10.11	11.05	0.05	4.14	3.77	0.08	6.52	0.83	**0.18**
KBB-013	5.19	57.90	0.41	11.16	10.27	0.03	3.35	2.64	0.09	7.00	0.97	**0.17**
KBB-014	4.50	58.59	0.43	11.10	11.74	0.01	3.06	1.21	0.05	7.46	0.51	0.08
KBB-015	4.96	53.73	0.14	9.00	18.62	0.01	3.68	0.93	0.03	7.66	0.30	0.09
KBB-016	4.98	53.24	0.11	8.69	19.76	0.01	3.60	0.71	0.01	7.81	0.28	0.06
KBB-017	8.36	45.65	0.09	7.38	26.26	0.00	3.00	0.67	0.04	6.68	0.22	0.31
KBB-018	4.72	54.10	0.12	8.50	18.93	0.01	3.41	1.10	0.03	7.59	0.48	0.06
KBB-019	4.82	54.23	0.16	9.05	18.42	0.01	3.38	0.88	0.03	7.74	0.34	0.05

Appendix 3. XRF pellet analysis raw results

XRF pellet																														
Sample	S (%)	Cl (%)	As (PPM)	Ba (PPM)	Br (PPM)	Ce (PPM)	veski Co (PPM)	Cr (PPM)	Cu (PPM)	F (%)	Ga (PPM)	La (PPM)	Mo (PPM)	Nb (PPM)	Ni (PPM)	Pb (PPM)	Rb (PPM)	Se (PPM)	Sr (PPM)	Th (PPM)	U (PPM)	V (PPM)	veski W (PPM)	Y (PPM)	Zn (PPM)	Zr (PPM)				
KB825-001	0.06	0.022	2.7	131.0	1.6	119.5	39.5	49.0	10.2	0.3	10.6	45.5	1.3	10.7	7.7	2.8	111.4	0.0	177.1	14.7	6.0	46.0	422.7	69.0	17.1	64.1				
KB825-002	0.09	0.051	1.6	60.8	4.6	86.1	40.4	43.3	7.4	0.2	6.9	25.1	1.2	6.1	3.6	6.9	75.4	0.0	127.9	14.6	5.0	27.5	370.9	52.3	9.0	45.6				
KB825-003	0.06	0.022	1.5	149.2	2.5	100.6	23.8	68.3	10.7	0.2	14.0	33.6	0.9	12.5	8.6	3.8	123.7	0.0	139.1	19.0	6.8	49.4	222.5	51.7	19.7	92.1				
KB825-004	0.16	0.032	2.9	66.0	2.5	90.7	32.8	59.4	14.5	0.4	10.0	32.5	2.5	4.5	17.5	5.6	90.0	0.0	153.2	11.9	15.6	40.5	241.2	55.0	12.3	110.0				
KB825-005	0.17	0.039	1.3	57.0	2.7	60.3	25.0	60.3	8.4	0.2	12.5	24.7	1.8	3.1	17.1	5.4	86.7	0.0	86.6	9.7	2.0	39.7	205.3	43.0	13.8	121.0				
KB825-006	0.09	0.043	3.2	93.5	3.0	45.9	14.8	35.6	9.9	0.1	9.4	26.6	1.0	3.4	14.7	1.1	67.5	0.0	77.1	4.3	0.0	34.1	130.4	40.4	16.0	54.6				
KB825-007	0.05	0.014	1.9	94.5	1.3	95.6	14.5	108.4	7.9	0.2	16.7	38.0	2.8	5.4	9.3	4.1	144.9	0.0	146.3	23.1	6.2	69.0	183.1	52.6	17.8	96.1				
KB825-008	0.03	0.009	3.0	109.6	0.6	65.8	19.1	140.2	9.5	0.2	24.1	24.1	2.1	6.0	9.7	0.0	184.4	0.0	121.5	15.8	7.1	85.6	161.1	38.0	26.0	108.3				
KB825-009	0.03	0.007	3.9	130.0	3.3	60.3	22.8	138.2	11.6	0.2	25.0	22.0	1.1	6.1	13.3	5.5	190.8	0.0	110.3	12.5	2.6	87.7	134.4	33.3	25.8	121.8				
KB825-010	0.07	0.008	2.2	128.4	1.3	70.6	23.2	130.7	13.5	0.2	21.9	26.3	2.0	3.9	11.6	1.8	186.5	0.3	117.6	14.8	7.5	89.1	118.0	40.0	25.9	105.0				
KB825-011	0.06	0.010	0.9	106.6	2.1	57.3	16.2	127.8	11.6	0.2	22.0	26.8	3.6	5.7	10.6	4.6	176.0	0.0	111.0	11.8	1.9	89.0	101.2	39.2	25.5	86.8				
KB825-012	0.16	0.009	8.6	117.2	0.3	53.1	15.4	130.8	12.9	0.2	22.6	32.8	2.3	6.5	14.7	4.0	182.1	0.0	106.7	13.8	2.1	97.1	120.5	35.6	26.9	96.6				
KB825-013	0.16	0.008	3.5	166.6	0.1	81.7	13.3	128.9	11.8	0.2	23.9	34.1	2.3	7.7	15.4	7.8	187.5	0.0	126.6	15.2	5.1	99.9	114.3	41.9	30.3	106.3				
KB825-014	**0.18**	0.005	7.2	170.3	0.6	52.8	24.8	125.0	13.4	0.1	24.1	29.5	2.0	8.5	19.1	5.0	204.7	0.1	82.2	13.2	3.2	92.7	110.5	24.6	33.1	104.7				
KB825-015	**0.15**	0.005	5.9	32.4	0.0	10.6	16.9	110.4	13.3	0.1	36.3	8.7	1.6	2.5	17.1	6.5	248.5	0.0	47.1	2.8	2.6	78.0	84.0	8.1	30.6	38.8				
KB825-016	**0.18**	0.006	23.6	29.4	0.6	14.5	15.9	103.7	13.0	0.1	37.8	1.9	2.3	2.1	19.5	2.1	257.4	0.0	46.5	5.6	4.4	64.7	65.5	8.5	31.1	20.2				
KB825-017	**7.8**	0.005	319.9	25.6	1.4	14.0	25.5	93.6	17.2	0.0	34.1	10.4	74.7	3.1	32.2	1.1	227.5	0.0	41.5	-0.5	1.5	61.7	79.7	3.9	30.5	18.0				
KB825-018	**0.08**	0.006	1.9	36.2	0.0	16.4	22.8	87.3	14.0	0.1	36.1	6.8	3.4	2.9	13.1	3.8	250.4	2.4	61.4	4.6	3.5	83.9	66.6	10.8	30.2	32.5				
KB825-019	**0.12**	0.004	2.3	74.6	0.1	8.2	17.7	81.4	20.3	0.1	36.4	13.0	4.0	4.0	22.4	1.7	248.0	0.0	53.6	5.1	5.0	114.4	58.7	6.7	30.6	47.1				

Annex
to Rector's directive No. 1-8/17 of 7 April 2020

Non-exclusive licence for reproduction and publication of a graduation thesis[1]

I, Kirke Britt Benjamin,

1. Grant Tallinn University of Technology free licence (non-exclusive licence) for my thesis

"Characteristics and Origin of Glauconite in Drillcore PH010B from the Toolse Phosphorite Deposit, Leetse Formation"

Supervised by Rutt Hints,

1.1 to be reproduced for the purposes of preservation and electronic publication of the graduation thesis, incl. to be entered in the digital collection of the library of Tallinn University of Technology until expiry of the term of copyright;

1.2 to be published via the web of Tallinn University of Technology, incl. to be entered in the digital collection of the library of Tallinn University of Technology until expiry of the term of copyright.

2. I am aware that the author also retains the rights specified in clause 1 of the non-exclusive licence.

3. I confirm that granting the non-exclusive licence does not infringe other persons' intellectual property rights, the rights arising from the Personal Data Protection Act or rights arising from other legislation.

25.05.2026
/ Signed digitally /

[1] *The non-exclusive licence is not valid during the validity of access restriction indicated in the student's application for restriction on access to the graduation thesis that has been signed by the school's dean, except in case of the university's right to reproduce the thesis for preservation purposes only. If a graduation thesis is based on the joint creative activity of two or more persons and the co-author(s) has/have not granted, by the set deadline, the student defending his/her graduation thesis consent to reproduce and publish the graduation thesis in compliance with clauses 1.1 and 1.2 of the non-exclusive licence, the non-exclusive license shall not be valid for the period.*